

Density Matrix Renormalization Group simulations of the SU(N) Fermi-Hubbard chain implementing the full SU(N) symmetry via Semi-Standard Young Tableaux and Unitary Group Subduction Coefficients.

Pierre Nataf¹

¹*Laboratoire de Physique et Modélisation des Milieux Condensés,
Université Grenoble Alpes and CNRS, 25 avenue des Martyrs, 38042 Grenoble, France*

(Dated: December 19, 2024)

We have developed an efficient method for performing density matrix renormalization group (DMRG) simulations of the SU(N) Fermi-Hubbard chain with open boundary conditions, fully leveraging the SU(N) symmetry of the problem. This method extends a previously developed approach for the SU(N) Heisenberg model and relies on the systematic use of the semi-standard Young tableaux (SSYT) basis in a DMRG algorithm "à la White". Specifically, the method aligns the site-by-site growth process of the infinite-size part of the DMRG, in its original formulation, with the site-by-site construction of the SSYT (or Gelfand-like) basis, based on the chain of unitary subgroups $U(1) \subset U(2) \subset U(3) \subset U(4) \dots$. We give special emphasis to the calculation of the symmetry-resolved reduced matrix elements of the hopping terms between the left and the right block, which makes direct use of the basis of SSYT and of the Gelfand-Tsetlin coefficients, offering a computational advantage in scaling with N compared to alternative methods that rely on summing over Clebsch-Gordan coefficients. Focusing on the model with homogeneous hopping between nearest neighbors, we have calculated the ground state energy as a function of U , i.e the atom-atom interaction amplitude, up to $N = 6$ for filling $1/N$ (one particle per site in average), and for one atom (resp. hole) away from filling $1/N$, allowing us to compute the charge gaps, and to estimate in the thermodynamical limit, the critical value U_c , separating the Mott insulator from the metallic phase. Central charges c are also extracted from the entanglement entropy using the Calabrese-Cardy formula, and are consistent with the theoretical predictions: $c = N - 1$, expected from the $SU(N)_1$ Wess-Zumino-Witten CFTs in the spin sector for the Mott phase, and $c = N$ in the metallic phase, reflecting the presence of one additional (charge) gapless critical mode.

I. INTRODUCTION

Recent advancements in ultracold atoms have enabled experimentalists to model strongly correlated systems with increasing precision and sophistication.¹⁻³ For example, degenerate gases of strontium and ytterbium loaded in optical lattices have been used to engineer the SU(N) Fermi-Hubbard models (FHM).⁴⁻¹² This is a generalization of the famous SU(2) FHM, which is crucial for the understanding of high-temperature superconductors and other quantum materials.¹³⁻¹⁷ Such a generalization, first introduced as a theoretical tool to provide us with an approximation scheme valid in the large N limit,¹⁸⁻²¹ was later explored at finite N in condensed matter, for, e.g., the study of some transition metal oxides,^{22,23} graphene's SU(4) spin valley symmetry,²⁴ Moiré bilayer graphene²⁵ and in cold atoms (resp. molecules) on optical lattices,²⁶⁻³³ where N can be as large as 10 (resp. 36), and where the SU(N) symmetry is (quasi-)exact. In the quest to identify conditions under which these systems could host exotic phases, extending their SU(2) counterparts, such as SU(N) chiral spin liquids in two-dimensional system^{25,34-41} or SU(N) Symmetry Protected Phase in one dimensional systems,⁴²⁻⁵⁰ theoreticians have quickly encountered some challenges.

In fact, for most of the SU(N) models, there is no reliable analytical treatment. Important exceptions are provided by the SU(N) Heisenberg (resp. FHM) Hamiltonian with uniform interaction (resp. hopping) between nearest neighbors on a chain, for which Sutherland⁵¹ (resp. Lieb and Wu⁵²) found the Bethe ansatz solution for any N (resp. $N = 2$).

Otherwise, theoreticians should rely on numerical methods,

and except in the cases where there is no sign problem so that they can use Quantum Monte Carlo,⁵³⁻⁵⁸ they must often struggle against the explosion of the size of the Hilbert space, so that they are either limited to very small system sizes, either limited to small N ($N = 5$ being often already considered as large). In fact, for the SU(N) FHM, for each added fermion, the dimension of the full Hilbert space is multiplied by 2^N , which already gives 64 for the (experimentally relevant) SU(6) fermions.

One strategy developed to overcome this difficulty is to implement the full SU(N) symmetry, which consists in working not in the full Hilbert space, but in a SU(N) symmetric sector invariant under the Hamiltonian, and corresponding to an SU(N) irreducible representation (irrep), usually labelled by a Young Diagram (YD).⁵⁹⁻⁶¹ It leads to a dramatic reduction of the number of linearly independent many-body wave-functions over which one should look for the states of smallest energies of the Hamiltonian. For instance, for the exact diagonalization (ED) of the Heisenberg SU(6) model on a $L = 12$ -sites lattice, for the fundamental irrep at each site (of dimension $N = 6$ since there are $N = 6$ flavors), the dimension of the full Hilbert space is $N^L \equiv 6^{12} \approx 2 \times 10^9$, while the dimension of the SU(6) singlet subspace (i.e the sector made of wave-functions invariant under local SU(6) transformations), is only 132,⁶² several order of magnitudes less. For the SU(6) FHM at filling $f = 1/6$, on the same $L = 12$ -sites cluster, going into the SU(6) singlets subspace is even more profitable, with a reduction of 13 orders of magnitudes⁶³!

Interpreting the Hamiltonian of the SU(N) FHM (resp. Heisenberg model) as an element of the algebra of the unitary (resp. permutation) group, we were able to implement

the $SU(N)$ symmetry in an ED algorithm using as a convenient basis, the set of semi-standard Young tableaux^{63,64} (resp. standard Young tableaux⁶²). In this framework, the algebra of a group is seen as a part of a chain of subalgebras with natural embedding.⁶⁵ For S_L , the group of permutations of L elements (L is the number of sites of the cluster under consideration), the embedding:

$$S_1 \subset S_2 \subset S_3 \subset \dots \subset S_{L-1} \subset S_L, \quad (1)$$

is at the heart of the construction (by A. Young^{59,66}) of the basis of standard Young tableaux (SYT) for the irrep of the permutation group, and of the calculation of the matrix elements of the elementary generators of the permutation group (i.e permutation between consecutive k for $1 \leq k \leq L$).

There is an interesting structural analogy between this site-after-site construction and the site-after-site growing process of the blocks in the Density Matrix Renormalization Group (DMRG) algorithm^{68,69} in the S. White's original formulation (cf. Fig 1), that we took advantage of in,⁶⁷ to implement the full $SU(N)$ symmetry in a DMRG algorithm. Such an implementation allowed us to bypass the calculation (and the painful storage) of the $SU(N)$ Clebsch-Gordan coefficients,⁷⁰ and to address relatively large L (up to several hundreds), and large N (up to $N = 8$), with good precision (6 to 12 digits, depending on N) for the ground state energies of the Heisenberg $SU(N)$ model on a chain with fundamental irrep on each site, as compared to the Bethe ansatz solutions, with $m = 1000$ states kept.⁶⁷ It also allowed us to solve some open physical problems around the numerical demonstration of the generalization of the Haldane's conjecture^{71,72} to $SU(3)$.^{19,73-79} In particular, we numerically proved⁸⁰ that the Heisenberg model with a two-boxes symmetric irrep at each site (of dimension 6) belongs to the universality class of the $SU(3)_1$ Wess-Zumino-Witten (WZW) conformal field theory (CFT)^{19,77,81-83} in agreement with the field theory predictions,⁸⁴ and we demonstrated using intensive DMRG simulations⁸⁵ that the model with a three-boxes symmetric irrep at each site (of dimension 10) was gapped.⁸⁶ In this latter case, by extrapolating our finite-size results, we were also able to obtain a 6-digits value for the ground state energy in the thermodynamical limit, which was later confirmed (on top of the presence of the gap)⁸⁷ with variational uniform matrix product states (VUMPS).⁸⁸

It is the purpose of the present paper to generalize those ideas to the $SU(N)$ FHM, to have a DMRG algorithm to address the FHM on chains with the full $SU(N)$ symmetry. Our protocol will be based on the embedding for the unitary groups:⁶⁵

$$U(1) \subset U(2) \subset U(3) \subset \dots \subset U(L-1) \subset U(L), \quad (2)$$

which allowed Gelfand and Tsetlin to build the representation of the unitary group in the basis of what is now called Gelfand-Tsetlin patterns,⁸⁹ which are equivalent to the semi-standard Young tableaux (SSYT), that we have used in⁶³ for ED. Given their clear analogy (cf Fig. 1), the previous code for the Heisenberg model should serve as a guideline, and we shall just highlight the differences.

The paper is organized as follows.

In section II, we describe the structure of the DMRG code which is based on the original formulation of DMRG by S. White,⁶⁸ and which relies on symmetry-resolved (multiplets) states written in the basis of SSYT for the implementation of the $SU(N)$ symmetry. In particular, a full part (cf subsection II C) is devoted to the calculation of the hopping term between the left and the right block, which makes use of the subduction coefficients for the unitary groups.⁶¹

In section III, we apply our formalism to the one-dimensional $SU(N)$ FHM with one particle per site on average (filling $1/N$), with uniform hopping between nearest neighbors and with open boundary conditions (OBC), but many of the concepts developed here can be generalized to other models. By also addressing the chain with one particle (resp. hole), away from filling $1/N$, we are able to calculate the charge gaps, to evaluate the critical value U_c separating the metallic from the insulating phase for $N = 3, 4$ and $N = 6$. We also calculate the entanglement entropy and the central charges and demonstrate some good agreement with the expected $SU(N)_1$ CFT behavior for the spin sector, with the presence of an additional critical mode in the metallic phase for $0 \leq U < U_c$.⁹⁰ Finally, conclusions and perspectives are drawn.

II. DMRG WITH IMPLEMENTATION OF THE FULL $SU(N)$ SYMMETRY

A. Model and Structure of the DMRG code

We describe here the DMRG algorithm that we use to study the $SU(N)$ Fermi-Hubbard model (FHM) whose Hamiltonian is:

$$H = \sum_{\langle i,j \rangle} \left(-t_{ij} E_{i,j} + \text{h.c.} \right) + \sum_{i=1}^L \frac{U_i}{2} E_{ii}^2, \quad (3)$$

where the $SU(N)$ invariant hopping terms read

$$E_{i,j} = E_{j,i}^\dagger = \sum_{\sigma=1}^N c_{i,\sigma}^\dagger c_{j,\sigma}, \quad (4)$$

where the σ are the color (or flavors) indexes. The t_{ij} in Eq. (3) are the hopping amplitudes between sites i and j and U_i is the local on-site density-density interaction for site $i = 1 \dots L$. For the numerical applications in the section III, we will consider uniform hoppings between nearest neighbors: $t_{ij} \equiv t > 0$ if $j = i + 1$ (and $t_{ij} = 0$ if $|i - j| > 1$), and with uniform positive interaction $U_i \equiv U > 0 \forall i = 1 \dots L$, but non uniform parameters could be implemented within the very same code. We will focus on a L -sites one-dimensional chain with OBC (cf Fig. 2), but the algorithm developed below could be adapted to other geometries or hoppings (rings, ladders, hoppings between next-nearest neighbors, etc...).

To implement the full $SU(N)$ symmetry to address the $SU(N)$ FHM, we use the basis of SSYT and the Gelfand-Tsetlin rules for the irreps of the unitary group,⁶³ in a way

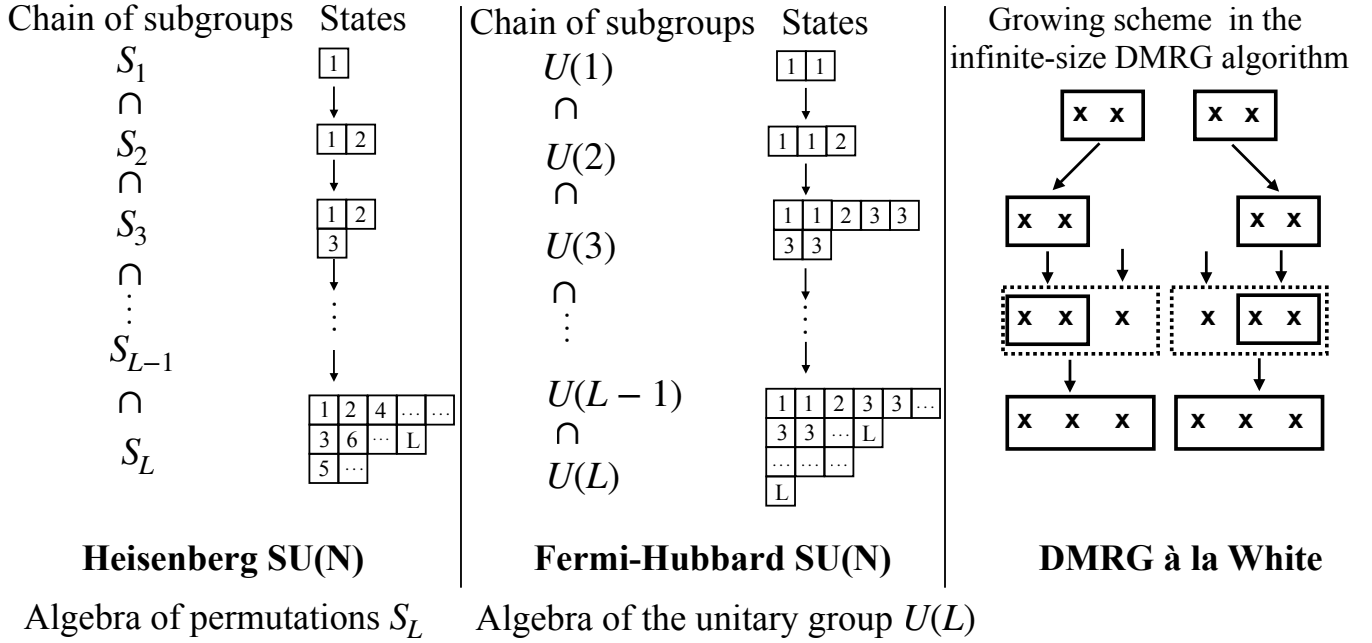


FIG. 1. Analogy between the site after site construction of the SU(N) symmetry-resolved states relevant for the Heisenberg SU(N) model (left),⁶⁷ the Fermi-Hubbard model (middle),⁶³ and with the site after site growing process in the original version of the Density Matrix Renormalization Group (DMRG⁶⁸) à la White (right).

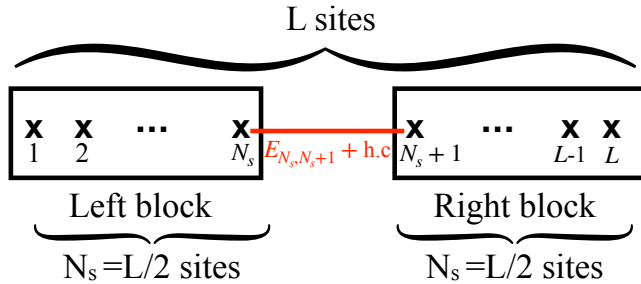


FIG. 2. System under consideration: open chain with $L = 2N_s$ sites. N_s is the number of sites of both the left and the right blocks which interact through the hermitian hopping $E_{N_s, N_s+1} + E_{N_s+1, N_s}$ where N_s is the index of the site at the very right (resp. left) of the left (resp. right) block.

that is similar to the protocole developed for the DMRG simulations of the SU(N) Heisenberg with SYT.⁶⁷ To illustrate our method, we focus on the infinite size part of the DMRG in the White's formulation: the chain is divided into the left and the right block, (cf Fig. 2). Each block is incrementally grown from size $N_s = L/2$ to size $N_s + 1$ (see Fig. 2), and to prevent the Hilbert space from becoming too large, we perform a density matrix truncation on both the irreps for each block, and on the states within each irrep. This ensures that the total number of states retained in each block does not exceed m , an input parameter (typically m is several thousands in section III). For this growth process, we detail below the selection of the states, the construction of the new matrices for the left (or

right) block, the creation of the superblock matrix, and finally the preparation for the next stage.

For the creation of the superblock, one needs in particular to calculate the reduced matrix elements (RME) for the interaction between the two blocks: $E_{N_s+1, N_s+2} + h.c.$, which is the step where the use of the SSYT is crucial: this is why a full subsection (cf subsection II C) is dedicated to this part, which is the key element of our methodological paper. The other parts, are more straightforward and rely primarily on a careful bookkeeping; we focus below on the modifications required for studying the SU(N) FHM compared to the SU(N) Heisenberg model⁶⁷ (mainly due to the occupation number which is not fixed any more on each site). Thus, a quick review the previous article⁶⁷ may also be useful, although the current paper is self-contained.

B. Description of one step of the infinite DMRG

An SU(N) irrep is *a priori* represented as an $N - 1$ rows Young Diagram (YD) $\alpha = [\alpha_1, \alpha_2, \dots, \alpha_{N-1}]$ with α_i the length of the i^{th} row of the shape α (cf Fig. 3 a for some examples of SU(3) YDs).⁵⁹⁻⁶¹ They can be characterized by the quadratic Casimir C_2 which depends on the shape of the SU(N) irrep α as:^{64,91}

$$C_2 = \frac{1}{2} \left\{ n(N - \frac{n}{N}) + \sum_{i=1}^{N-1} \alpha_i^2 - \sum_{j=1}^{j=\alpha_1} \bar{\alpha}_j^2 \right\}, \quad (5)$$

where the α_i ($i = 1, \dots, N - 1$) are the lengths of the rows and the $\bar{\alpha}_j$ ($j = 1, \dots, \alpha_1$) are the lengths of the columns, and

n is the number of boxes of the irrep. A $SU(N)$ irrep represents a sector in the Hilbert space containing many-body states which behave the same way under local $SU(N)$ transformations. When we add or withdraw a N -boxes column to a YD (from the left), it still represents the same $SU(N)$ irrep, but it is useful when dealing with diagrammatic representation of $SU(N)$ states (or multiplets) like the SYT or the SSYT to choose the convention where there are as many fermions as boxes in the YD (cf Fig. 3 b).

In our algorithm, like in,⁶⁷ we make a truncation over the $SU(N)$ irreps: only the states living in the M irreps of lowest quadratic Casimir C_2 (cf Eq. 5) will be considered (cf Fig. 3 a), where M is an input parameter of the simulations (typically $M = 300$ to 420 in section III). This is physically relevant for the antiferromagnetic phases, but may present challenges in the case of a ferromagnet or in the metallic phases: there, the convergence with the physical parameters shall be carefully controlled. A benefit from this truncation is that the number of required group theory coefficients is finite, and can be computed once for all before running the simulations.

In addition, there are constraints on the shapes for the possible irreps at stage N_s : for a block of size N_s sites, one can not have $SU(N)$ YD with more than N_s columns since we have fermions in the system, and more than $f \times NL$ boxes which is the total number of particles for the full chain, where f is the filling (one input of the algorithm) and $L = 2N_s$ the number of sites of the entire chain. Finally, as shown in,^{63,64} in order to use the basis of SSYT for a given set of $SU(N)$ fermions on N_s sites, one should *transpose* the shapes $\alpha \rightarrow \bar{\alpha}$ (i.e transforming the rows into columns and columns into rows), to consider the shapes $\bar{\alpha}$ as $U(N_s)$ irreps. Then, the constraints over the maximal number of rows/columns are transposed accordingly (cf Fig. 3 and Fig. 4).

1. Selection of states for the current step and construction of the new matrices for the left block

We explain here how to pass from the stage where both the *left* and the *right* blocks have N_s sites to the stage where they both have $N_s + 1$ sites. Focusing on the left block, we assume that we have kept in memory $m_{N_s} \leq m$ states from the previous stage, each of them belonging to a given $SU(N)$ symmetry sector $\bar{\alpha}$ (seen as an $U(N_s)$ irrep).

$$\{|\zeta_1^{\bar{\alpha}}\rangle, |\zeta_2^{\bar{\alpha}}\rangle, \dots, |\zeta_{m_{N_s}}^{\bar{\alpha}}\rangle\}. \quad (6)$$

The number of states $m_{N_s}^{\bar{\alpha}}$ satisfy:

$$\sum_{\bar{\alpha}} m_{N_s}^{\bar{\alpha}} = m_{N_s}, \quad (7)$$

where the sum runs over the shapes $\bar{\alpha}$ satisfying the constraints for the number of rows/columns/boxes explained above.

The states in Eq. (6) are the eigenstates of the $m_{N_s}^{\bar{\alpha}} \times m_{N_s}^{\bar{\alpha}}$ reduced density matrix $\rho^{\bar{\alpha}}$ (we will show later how to calculate the reduced density matrix for a given sector $\bar{\alpha}$). The corresponding positive eigenvalues are ranked from the largest to

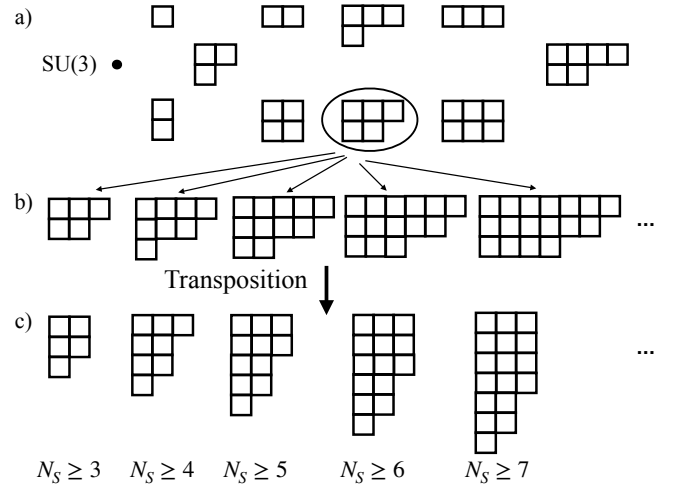


FIG. 3. a) Example of the truncation: we select the first $M = 11$ $SU(3)$ irreps according to the quadratic Casimir. b) Equivalence of $SU(N)$ irreps (here $[3\ 2]$ for $SU(3)$) modulo added/withdrawn N -boxes columns. One can always choose the representation of an $SU(N)$ irrep through a Young Diagram with as much box as $SU(N)$ fermions. c) When transposed (rows changed into columns, and columns into rows), the YD represents an $U(N_s)$ irrep, where N_s is the number of sites of each block, with at most N columns and N_s rows.

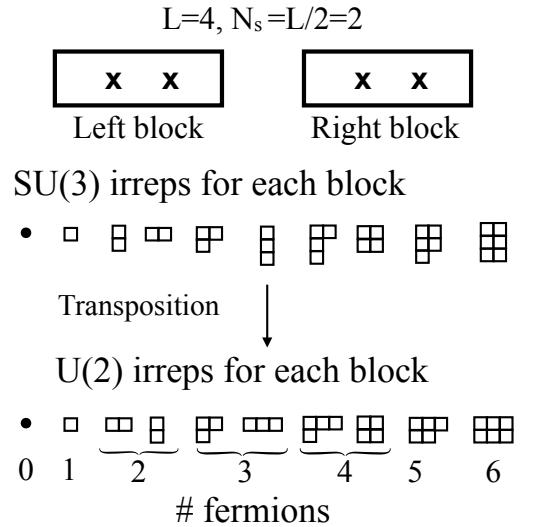


FIG. 4. Example of $SU(N=3)$ irreps for each block of size $N_s = L/2 = 2$ ($L = 4$ sites in the full chain). The shapes of the $SU(N)$ (resp. $U(N_s)$) irreps are constrained to have at most N rows (resp. columns) and N_s columns (resp. rows). The number of box in each irrep is equal to the number of $SU(N)$ fermions in each block.

the lowest: $\{\lambda_1^{\bar{\alpha}}, \lambda_2^{\bar{\alpha}}, \dots, \lambda_{m_{N_s}}^{\bar{\alpha}}\}$. In addition, we also assume that from the previous stage we have kept the matrices $\mathcal{H}_{N_s}^{\bar{\alpha}}$, which are the matrices of the FHM H_{N_s} with OBC for N_s sites, expressed in the basis of Eq. (6): the (i, j) coefficient of $\mathcal{H}_{N_s}^{\bar{\alpha}}$ is $(\mathcal{H}_{N_s}^{\bar{\alpha}})_{i,j} = \langle \zeta_i^{\bar{\alpha}} | H_{N_s} | \zeta_j^{\bar{\alpha}} \rangle$.

To add a new site and select $m_{N_s+1} \leq m$ states, we scruti-

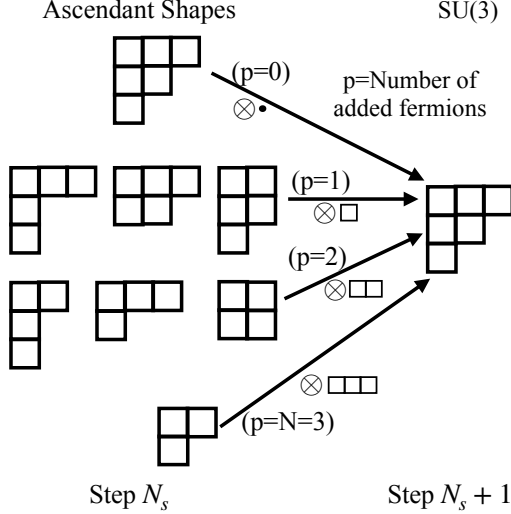


FIG. 5. We show here examples of *ascendant* shapes $\bar{\alpha}$ (on the left) for the shape $\bar{\beta} = [321]$ for $N = 3$. $\bar{\beta}$ should belong to $\bar{\alpha} \otimes [p]$ ($p = 0, 1, \dots, N$), where $[p]$ is the one-row fully symmetric irrep with p boxes. See text for details.

nize every shape $\bar{\beta}$ which satisfies the constraints (i.e less than $N_s + 1$ rows, N columns and $f \times N(2N_s + 2)$ boxes), and is equivalent (after transposition) to one of the M input $SU(N)$ irreps. There are M_{N_s+1} such shapes. For each shape $\bar{\beta}$, we consider all the possible *ascendant* shapes $\bar{\alpha}$: they are such that $\bar{\beta}$ belongs to the tensor product $\bar{\alpha} \otimes [p]$ for $p = 0, 1, \dots, N$, where $[p]$ is the one-row fully symmetric irrep of p boxes, which is the transpose of the p -box single column irrep, which is the irrep of the added single site with p fermions on it (See Fig. 5 for an $SU(3)$ example).

Like in,⁶⁷ for every shape $\bar{\beta}$, we create $L_{\bar{\beta}}$, the list containing all the eigenvalues $\lambda_q^{\bar{\alpha}}$ of all the associated ascendant shapes $\bar{\alpha}$, and we create then L_{N_s+1} , the union of these lists $L_{N_s+1} = \cup_{\bar{\beta}} L_{\bar{\beta}}$. We choose the m_{N_s+1} largest values in L_{N_s+1} , where $m_{N_s+1} = \text{Min}(m, \text{cardinal}(L_{N_s+1}))$, and the labels attached to each of the chosen $\lambda_q^{\bar{\alpha}}$ allows one to select for each sector $\bar{\beta}$ and each ascendant shape $\bar{\alpha}$, $m_{\bar{\beta}, N_s+1}^{\bar{\alpha}}$ ascendant states, so that $m_{N_s+1}^{\bar{\beta}} = \sum_{\bar{\alpha}} m_{\bar{\beta}, N_s+1}^{\bar{\alpha}}$ will be the dimension of the subspace corresponding to the irrep $\bar{\beta}$ in the left (or right) block of size $N_s + 1$. Calling σ_{β} the sum of the corresponding eigenvalues, the weight discarded by the current selection (truncation) is $\mathcal{W}_d^{m,L} = 1 - \sum_{\beta} g_{\beta} \sigma_{\beta}$, where $g_{\beta} = \text{dim}(\beta)/h$, with $\text{dim}(\beta)$, the dimension of the $SU(N)$ irrep of shape β (before transposition), and where h is the dimension of the local Hilbert space, i.e. $h = 2^N$. Note that for the Heisenberg model with the fundamental $SU(N)$ irrep on each site, the same formula applied but with $h = N$.⁶⁷

In addition, the set of numbers $\{m_{\bar{\beta}, N_s+1}^{\bar{\alpha}}\}_{\bar{\alpha}}$ (stage $N_s + 1$) and $\{m_{\bar{\alpha}, N_s}^{\bar{\chi}}\}_{\bar{\chi}}$ (stage N_s), define a genealogy for each state in the sector $\bar{\beta}$ up to the *grandparent* level. These set of numbers, and the set of wave-functions $\{|\zeta_1^{\bar{\alpha}}\rangle, |\zeta_2^{\bar{\alpha}}\rangle, \dots, |\zeta_{m_{\bar{\beta}, N_s}^{\bar{\alpha}}}^{\bar{\alpha}}\rangle\}$,

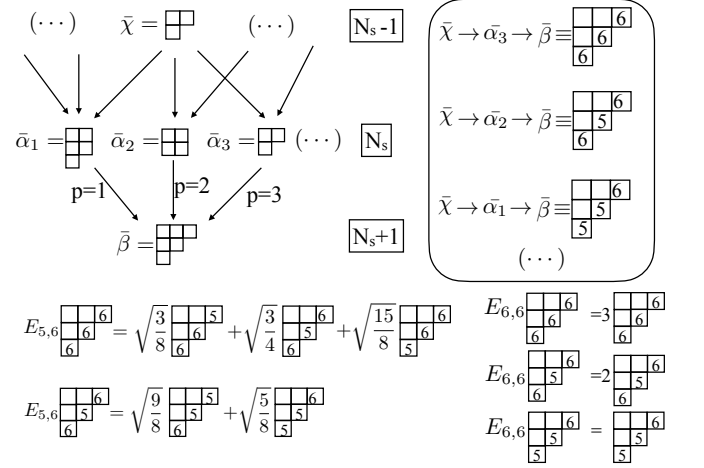


FIG. 6. To create $E_{N_s, N_s+1} + h.c$ and E_{N_s+1, N_s+1} on the sector labelled by a shape $\bar{\beta}$, one just needs to know the chain of shapes $\bar{\chi} \rightarrow \bar{\alpha} \rightarrow \bar{\beta}$ which characterize the different class of states, as it determines the locations and the number of occurrences of the numbers N_s and $N_s + 1$ on each SSYT ($N_s = 5$ here). In particular, p designates in this figure the number of occurrences of $N_s + 1$ in the SSYT, and also the number of added fermions on the site $N_s + 1$. We apply the Gelfand-Tsetlin rules⁸⁹ (cf the appendix of⁶³) to obtain the coefficients of the generators E_{N_s, N_s+1} and E_{N_s+1, N_s+1} on each class of states. See text for details.

$\forall \bar{\alpha}$ an ascendant shape of $\bar{\beta}$, are the two sufficient ingredients, with the Gelfand-Tsetlin rules for the coefficients of the generators of $U(N_s + 1)$ (cf^{70,89,92} or the appendix of⁶³), to build the new matrices for the left block. In fact, the FHM Hamiltonian for $N_s + 1$ sites, can be decomposed as:

$$H_{N_s+1} = H_{N_s} - t(E_{N_s, N_s+1} + h.c) + \frac{U}{2} E_{N_s+1, N_s+1}^2. \quad (8)$$

First, the matrix representing H_{N_s} in the sector $\bar{\beta}$ (of size $m_{N_s+1}^{\bar{\beta}} \times m_{N_s+1}^{\bar{\beta}}$) is just the concatenation of the submatrices $(\mathcal{H}_{N_s}^{\bar{\alpha}})_{i,j}$ where $1 \leq i \leq m_{\bar{\beta}, N_s+1}^{\bar{\alpha}}, 1 \leq j \leq m_{\bar{\beta}, N_s+1}^{\bar{\alpha}}$, and where the matrices $\mathcal{H}_{N_s}^{\bar{\alpha}}$ were kept in memory from the previous stage.

Furthermore, the genealogy of each state in the sector $\bar{\beta}$, characterized by the chain of shapes $\bar{\chi} \rightarrow \bar{\alpha} \rightarrow \bar{\beta}$, is enough to calculate the matrices representing both E_{N_s+1, N_s+1} and E_{N_s, N_s+1} (and its h.c) on the sector $\bar{\beta}$, as it gives the locations (and the number of occurrences) of the indices N_s and $N_s + 1$ in the SSYTs, which form the underlying basis on which each state is decomposed. Firstly, as illustrated in Fig. 6, the part of the chain $\bar{\alpha} \rightarrow \bar{\beta}$ tells us how many boxes one adds from $\bar{\alpha}$ to $\bar{\beta}$, which is nothing but the number of fermions on site $N_s + 1$ (equal to the operator E_{N_s+1, N_s+1}), also equal to the number of occurrences of the index $N_s + 1$ in every SSYT. Secondly, for a matrix element $\langle \zeta_i^{\bar{\alpha}} | E_{N_s, N_s+1} | \zeta_j^{\bar{\alpha}'} \rangle$, not to be zero, the "grand father" shape $\bar{\chi}$ should be common, and the number of occurrences of $N_s + 1$ (resp. N_s) in the SSYT on which $|\zeta_j^{\bar{\alpha}'}\rangle$ is decomposed should be one more (resp. one less) than such

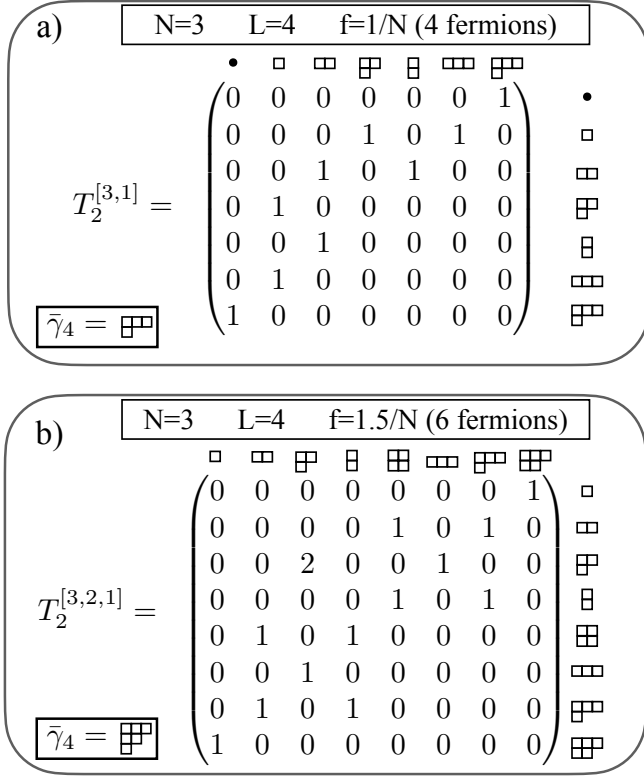


FIG. 7. Examples of shapes $\tilde{\gamma}_L$ representing some targeted irreps and matrices $T_{N_s+1}^{\tilde{\gamma}_L}$ for $N_s + 1 = 2$ ($L = 4$) for SU(3) and for the targeted irrep $\tilde{\gamma}_L = [31]$ in a), and for the targeted irrep $\tilde{\gamma}_L = [321]$ in b). The shapes β_q (resp. β'_q) for $q = 1, \dots, M_{N_s+1}$ which label the columns (resp. lines) of the matrices $T_2^{\tilde{\gamma}_L}$ are the transposed Young Diagram of the shapes representing the SU(N) irreps for the left (resp. for the right) block made of $N_s + 1 = L/2 (= 2)$ sites. Then, the entries $T_{N_s+1}^{\tilde{\gamma}_L}(q, q')$ are the multiplicities of $\tilde{\gamma}_L \in \tilde{\beta}_q \otimes \tilde{\beta}_{q'}$ (see text for details)

number in $|\zeta_i^{\tilde{\alpha}}\rangle$. The Gelfand-Tsetlin coefficients for the generators of the unitary group⁸⁹ (cf the appendix of⁶³) illustrated in Fig. 6, and proper overlap of vectors of coefficients (split according to the numbers $\{m_{\tilde{\alpha}, N_s}^{\tilde{\chi}}\}_{\tilde{\chi}}$), enable us to calculate the matrix representing E_{N_s, N_s+1} on the sector $\tilde{\beta}$.

2. Matrix for the superblock and preparation of the next stage

We calculate now the matrix representing the Hamiltonian H_L for the full chain which can be decomposed as:

$$H_L = H_{N_s+1}^{\text{Left}} + H_{N_s+1}^{\text{Right}} - t(E_{N_s+1, N_s+2} + h.c.), \quad (9)$$

where E_{N_s+1, N_s+2} is the hopping term from the very first site of the right block to the very last site of the left block (cf Fig. 2), and where $H_{N_s+1}^{\text{Left}}$ (resp. $H_{N_s+1}^{\text{Right}}$) is the Hamiltonian of the SU(N) FHM for the left (resp. right) block of size $N_s + 1$. We need to know on which targeted irrep $\tilde{\gamma}_L$ one wants to get the ground state of. It one targets the absolute ground state, it depends on the parameters of the problems, and one can perform

ED on small chains to have a general idea. For instance, for $U \gtrsim |t|$, and for filling $1/N$ (one particle per site on average), the ground state of the SU(N) FHM is antiferromagnetic, living in the SU(N) singlet irrep $\gamma_L = [L/N, L/N, \dots, L/N]$ (i.e. $\tilde{\gamma}_L = [N, N, \dots, N]$, with L/N rows) for L multiple of N , and in the most antisymmetric one otherwise.

To build the superblock, one first calculate the $M_{N_s+1} \times M_{N_s+1}$ matrix $T_{N_s+1}^{\tilde{\gamma}_L}$ whose coefficients $T_{N_s+1}^{\tilde{\gamma}_L}(q, q')$ are equal to the Outer Multiplicity of $\tilde{\gamma}_L$ in $\tilde{\beta}_q \otimes \tilde{\beta}_{q'}$, for $1 \leq q, q' \leq M_{N_s+1}$, and where the $\tilde{\beta}_q$ and $\tilde{\beta}_{q'}$ are among the M_{N_s+1} shapes $\tilde{\beta}$ for the left and right block. To perform such a tensor product, one can, for instance, use the Itzykson-Nauenberg rules,⁹³ also known as Littlewood Richardson rules. A good implementation of these rules is proposed p.15 of.⁷⁰ Note that when $\gamma_L \notin \tilde{\beta}_q \otimes \tilde{\beta}_{q'}$, $T_{N_s+1}^{\tilde{\gamma}_L}(q, q') = 0$. We give in Fig. 7 some instances of the matrix $T_{N_s+1}^{\tilde{\gamma}_L}$ for $N = 3$ for two different targeted irreps $\gamma_{L=4}$. We then list the $M_{N_s+1}^{GS} \leq M_{N_s+1}$ relevant shapes $\tilde{\beta}_k$ (for $1 \leq k \leq M_{N_s+1}$), which are such that the column $T_{N_s+1}^{\tilde{\gamma}_L}(:, k)$ have at least one non zero entry.

The Hilbert space of the superblock on the sector $\tilde{\gamma}_L$ is then the direct sum of the tensor product of the sectors corresponding to the shapes $\tilde{\beta}_k$ (for $k = 1, \dots, M_{N_s+1}^{GS}$) for the left block and the sector labelled by the shapes $\tilde{\beta}_{k'}$ for the right block with a multiplicity equal to $T_{N_s+1}^{\tilde{\gamma}_L}(k, k')$. Consequently, the matrices $\mathcal{H}_{N_s+1}^{\text{Left}}$ and $\mathcal{H}_{N_s+1}^{\text{Right}}$ representing respectively $H_{N_s+1}^{\text{Left}}$ and $H_{N_s+1}^{\text{Right}}$ on the sector γ_L of the superblock, are:

$$\mathcal{H}_{N_s+1}^{\text{Left}} = \bigoplus_{T_{N_s+1}^{\tilde{\gamma}_L}(q, q') > 0} \bigoplus_{r=1}^{T_{N_s+1}^{\tilde{\gamma}_L}(q, q')} \mathcal{H}_{N_s+1}^{\tilde{\beta}_q} \otimes \mathcal{I}_{N_s+1}^{\tilde{\beta}_{q'}}$$

$$\mathcal{H}_{N_s+1}^{\text{Right}} = \bigoplus_{T_{N_s+1}^{\tilde{\gamma}_L}(q', q) > 0} \bigoplus_{r=1}^{T_{N_s+1}^{\tilde{\gamma}_L}(q', q)} \mathcal{I}_{N_s+1}^{\tilde{\beta}_{q'}} \otimes \mathcal{H}_{N_s+1}^{\tilde{\beta}_q}, \quad (10)$$

where $\mathcal{I}_{N_s+1}^{\tilde{\beta}_q}$ is the $m_{N_s+1}^{\tilde{\beta}_q} \times m_{N_s+1}^{\tilde{\beta}_q}$ identity matrix on the sector labelled by the shape $\tilde{\beta}_q$ (for the left or the right blocks). The basis for the superblock is made of vectors of the form $|\zeta_i^{\tilde{\beta}_q}, \zeta_j^{\tilde{\beta}_{q'}}, r\rangle$, for $1 \leq r \leq T_{N_s+1}^{\tilde{\gamma}_L}(q, q')$, $1 \leq i \leq m_{N_s+1}^{\tilde{\beta}_q}$ and $1 \leq j \leq m_{N_s+1}^{\tilde{\beta}_{q'}}$, and the dimension of the superblock is thus $\sum_{q, q'} T_{N_s+1}^{\tilde{\gamma}_L}(q, q') \times m_{N_s+1}^{\tilde{\beta}_q} \times m_{N_s+1}^{\tilde{\beta}_{q'}}$. As for $E_{N_s+1, N_s+2}^{\tilde{\gamma}_L} + h.c.$, i.e., the matrix representing the hopping between the left and the right block on the targeted irrep, we devote the entire next section to it, with particular emphasis on the use of the subduction coefficients of the unitary group.

Finally, from $\mathcal{H}_L^{\tilde{\gamma}_L}$, i.e the matrix representing H_L on $\tilde{\gamma}_L$, one calculates the ground state $G_{\tilde{\gamma}_L}^L$, which is the eigenvector of minimal energy, using for instance the Lanczos algorithm. Then, calling V_i^k the vector of indices of every states of the form $|\zeta_i^{\tilde{\beta}_k}, \dots, \dots\rangle$ in the full Hilbert space, for $k = 1, \dots, M^{GS}$ and $1 \leq i \leq m_{N_s+1}^{\tilde{\beta}_k}$, one computes the reduced density matrices $\rho^{\tilde{\beta}_k}$, whose coefficients are (for $1 \leq i, j \leq$

$m_{N_s+1}^{\tilde{\beta}_k} \rho^{\tilde{\beta}_k}(i, j) = \dim(\tilde{\beta}_k^T)^{-1} G_{\tilde{\gamma}_L}^{L, \dagger}(V_i^k) G_{\tilde{\gamma}_L}^L(V_j^k)$, where $\dim(\tilde{\beta}_k^T)^{-1}$ is the inverse of the dimension of the SU(N) irrep of shape $\tilde{\beta}_k^T$ (which is the shape whose transposition gives $\tilde{\beta}_k$), and which guarantees the correct normalization of the reduced density matrices.

We then diagonalize the reduced density matrices to obtain the set of eigenvalues ranked from the largest to the lowest one: $\{\lambda_1^{\tilde{\beta}_k}, \lambda_2^{\tilde{\beta}_k}, \dots, \lambda_{m_{N_s+1}^{\tilde{\beta}_k}}^{\tilde{\beta}_k}\}$, as well as the corresponding eigenvectors: $\{|\zeta_1^{\tilde{\beta}_k}\rangle, |\zeta_2^{\tilde{\beta}_k}\rangle, \dots, |\zeta_{m_{N_s+1}^{\tilde{\beta}_k}}^{\tilde{\beta}_k}\rangle\}$, and we perform a rotation to reexpress $\mathcal{H}_{N_s+1}^{\tilde{\beta}_k}$ in this basis. We keep in memory those quantities for the next stage. At this step, one can also calculate the entanglement entropy $S(L)$:

$$S(L) = - \sum_{k=1}^{M_{N_s+1}^{G_S}} \dim(\tilde{\beta}_k) \rho^{\tilde{\beta}_k} \log(\rho^{\tilde{\beta}_k}), \quad (11)$$

where the coefficients $\dim(\tilde{\beta}_k)$ account for the multiplicities (cf^{67,94,95}). Note that the matrices representing the FHM in the irrelevant sectors, i.e.:

$$\mathcal{H}_{N_s+1}^{\tilde{\beta}} \text{ for } \tilde{\beta} \notin \{\tilde{\beta}_1, \tilde{\beta}_2, \dots, \tilde{\beta}_{M_{N_s+1}^{G_S}}\}$$

do not undergo any transformation at this step.

C. Calculation of the reduced matrix element for the interaction between the left and the right block.

In this section, we show how to calculate the matrix $E_{\tilde{\gamma}_L} \equiv E_{N_s+1, N_s+2}^{\tilde{\gamma}_L}$, which represents the hopping term from the very first site of the right block to the very last site of the left block, i.e. E_{N_s+1, N_s+2} on the sector $\tilde{\gamma}_L$.

First of all, for $\beta_{q_1}, \beta_{q_2}, \beta_{q_3}, \beta_{q_4} \in \{\tilde{\beta}_1, \tilde{\beta}_2, \dots, \tilde{\beta}_{M_{N_s+1}^{G_S}}\}$ and for i_j such that $1 \leq i_j \leq m_{N_s+1}^{\beta_{q_j}}$ (for $j = 1, \dots, 4$), the coefficients $\langle \eta_{i_3}^{\beta_{q_3}} | \langle \eta_{i_4}^{\beta_{q_4}} | E_{\tilde{\gamma}_L} | \eta_{i_1}^{\beta_{q_1}} \rangle \otimes | \eta_{i_2}^{\beta_{q_2}} \rangle$ will be zero unless that both $\tilde{\gamma}_L \in \beta_{q_1} \otimes \beta_{q_2}$ and $\tilde{\gamma}_L \in \beta_{q_3} \otimes \beta_{q_4}$, i.e. $T_{N_s+1}^{\tilde{\gamma}_L}(q_1, q_2), T_{N_s+1}^{\tilde{\gamma}_L}(q_3, q_4) > 0$

In addition, and analogously to the Heisenberg case, one can introduce the *shape and cross* notation for these coefficients, which keep track of the chain of sectors when making each block grow from N_s sites to $N_s + 1$ sites. In particular, we will go into detail on the following example which is useful for $N \geq 4$:

$$\begin{aligned} & \left\langle \begin{array}{|c|c|c|c|} \hline \square & \square & \square & \times \\ \hline \square & \square & \square & \square \\ \hline \square & \square & \square & \square \\ \hline \square & \square & \square & \square \\ \hline \end{array} \otimes \begin{array}{|c|c|c|c|} \hline \square & \square & \square & \square \\ \hline \square & \square & \square & \square \\ \hline \square & \square & \square & \square \\ \hline \square & \square & \square & \square \\ \hline \end{array} \left| E \right. \begin{array}{|c|c|c|c|} \hline \square & \square & \square & \square \\ \hline \square & \square & \square & \square \\ \hline \square & \square & \square & \square \\ \hline \square & \square & \square & \square \\ \hline \end{array} \left| \begin{array}{|c|c|c|c|} \hline \square & \square & \square & \square \\ \hline \square & \square & \square & \square \\ \hline \square & \square & \square & \square \\ \hline \square & \square & \square & \square \\ \hline \end{array} \otimes \begin{array}{|c|c|c|c|} \hline \square & \square & \square & \square \\ \hline \square & \square & \square & \square \\ \hline \square & \square & \square & \square \\ \hline \square & \square & \square & \square \\ \hline \end{array} \right\rangle \\ & = \frac{\sqrt{3}}{2\sqrt{2}} \end{aligned} \quad (12)$$

In the above example, $\tilde{\gamma}_L = [4, 4, 4, 3, 3]$, $\beta_{q_1} = [4, 3, 1]$, $\beta_{q_2} = [4, 3, 2, 1]$, $\beta_{q_3} = [4, 3, 2]$ and $\beta_{q_4} =$

$[4, 3, 1, 1]$. In such a notation, the shapes without (resp. with) the boxes containing the cross represent the irrep when each block has N_s (resp. $N_s + 1$) sites. Please note that in such an example, $\tilde{\gamma}_L$ appears with outer multiplicity equal to one in both $\beta_{q_1} \otimes \beta_{q_2}$ and in $\beta_{q_3} \otimes \beta_{q_4}$, i.e. $T_{N_s+1}^{\tilde{\gamma}_L}(q_1, q_2) = T_{N_s+1}^{\tilde{\gamma}_L}(q_3, q_4) = 1$, which will simplify the following treatment. However, the methodology we have developed is not restricted to outer multiplicity ≤ 1 , and we will discuss the situation where $T_{N_s+1}^{\tilde{\gamma}_L}(q_1, q_2) \cdot T_{N_s+1}^{\tilde{\gamma}_L}(q_3, q_4) > 1$ at the end of this section.

Furthermore, another condition for the above coefficient not to vanish is that when one withdraws a box containing a cross in β_{q_2} to add it to β_{q_1} , one should obtain respectively β_{q_4} and β_{q_3} with their cross located in the good position.

Finally, and as we will show, the value of the coefficient in Eq. 12 depends on the relative position of the cross for the left block with respect to the cross for the right block in the shape $\tilde{\gamma}_L$, so that empty N -boxes row could be safely deleted/added from the top in $\beta_{q_1}, \beta_{q_2}, \beta_{q_3}, \beta_{q_4}$ and $\tilde{\gamma}_L$ ⁹⁶. Thus, one has for instance:

$$\begin{aligned} & \left\langle \begin{array}{|c|c|c|c|} \hline \square & \square & \square & \square \\ \hline \square & \square & \square & \square \\ \hline \square & \square & \square & \square \\ \hline \square & \square & \square & \square \\ \hline \end{array} \otimes \begin{array}{|c|c|c|c|} \hline \square & \square & \square & \square \\ \hline \square & \square & \square & \square \\ \hline \square & \square & \square & \square \\ \hline \square & \square & \square & \square \\ \hline \end{array} \left| E \right. \begin{array}{|c|c|c|c|} \hline \square & \square & \square & \square \\ \hline \square & \square & \square & \square \\ \hline \square & \square & \square & \square \\ \hline \square & \square & \square & \square \\ \hline \end{array} \left| \begin{array}{|c|c|c|c|} \hline \square & \square & \square & \square \\ \hline \square & \square & \square & \square \\ \hline \square & \square & \square & \square \\ \hline \square & \square & \square & \square \\ \hline \end{array} \otimes \begin{array}{|c|c|c|c|} \hline \square & \square & \square & \square \\ \hline \square & \square & \square & \square \\ \hline \square & \square & \square & \square \\ \hline \square & \square & \square & \square \\ \hline \end{array} \right\rangle \\ & = \left\langle \begin{array}{|c|c|c|c|} \hline \square & \square & \square & \square \\ \hline \square & \square & \square & \square \\ \hline \square & \square & \square & \square \\ \hline \square & \square & \square & \square \\ \hline \end{array} \otimes \begin{array}{|c|c|c|c|} \hline \square & \square & \square & \square \\ \hline \square & \square & \square & \square \\ \hline \square & \square & \square & \square \\ \hline \square & \square & \square & \square \\ \hline \end{array} \left| E \right. \begin{array}{|c|c|c|c|} \hline \square & \square & \square & \square \\ \hline \square & \square & \square & \square \\ \hline \square & \square & \square & \square \\ \hline \square & \square & \square & \square \\ \hline \end{array} \left| \begin{array}{|c|c|c|c|} \hline \square & \square & \square & \square \\ \hline \square & \square & \square & \square \\ \hline \square & \square & \square & \square \\ \hline \square & \square & \square & \square \\ \hline \end{array} \otimes \begin{array}{|c|c|c|c|} \hline \square & \square & \square & \square \\ \hline \square & \square & \square & \square \\ \hline \square & \square & \square & \square \\ \hline \square & \square & \square & \square \\ \hline \end{array} \right\rangle \end{aligned} \quad (13)$$

This means that the number of such coefficients is finite when one considers only the M first SU(N) irreps. An upper boundary for this number of coefficients is $M \times 2^N \times 2^N \times N^2$. In fact, for a given shape, there are at most $\binom{N}{k}$ ways to locate k cross, for $k = 0, 1, \dots, N$, which gives a first factor 2^N . For each of these shape+cross, one has one partner shape such that the tensor product might give $\tilde{\gamma}_L$, with at most 2^N different configurations for the cross. Finally, given such a *ket*, one has at most N^2 ways to delete one cross in the right block shape to add it in the left block shape. Such a number is an overestimation by a factor N typically, so for $M = 300$, depending on $\tilde{\gamma}_L$, one has typically $\sim 10^7$ non zero coefficients for $N = 6$ and $\sim 10^5$ non zero coefficients for $N = 3$. One should store them before running the simulations.

1. Calculation of the reduced matrix elements using the $U(m+n) \supset U(m) \otimes U(n)$ subduction coefficients.

In this section, we will show how to calculate the coefficients $\langle \beta_{q_3}, l_3 | \otimes \langle \beta_{q_4}, l_4 | E_{\tilde{\gamma}_L} | \beta_{q_1}, l_1 \rangle \otimes | \beta_{q_2}, l_2 \rangle$, where β_{q_j} is a shape with at most N columns (i.e. transposition of SU(N) irrep or Young diagram), and l_j is the vector of rows (conventionally ranked in descending order) of the cross (or bottom corners⁹⁷) inside β_{q_j} , for $j = 1, 2, 3, 4$. We call n_j the length of the vector l_j , i.e the number of cross in the shape β_{q_j} for $j = 1, 2, 3, 4$. We will describe in detail the different steps to calculate this kind of coefficients, and we will apply them to the SU(4) example introduced above (cf Eq. (12)). The idea

is to use the SSYT's and the Gelfand-Tsetlin representation of the unitary group to compute this kind of coefficient.

Step 1

- We first replace the couple (β_{q_1}, l_1) by a SSYT S_1 of the same shape, having its last numbers (equal to $r_1 + 1$, where r_1 is the number of rows of the shape β_{q_1} without the cross) located in the bottom corners $l_1: (\beta_{q_1}, l_1) \rightarrow S_1$. For our example, $(\beta_{q_1}, l_1) = ([4, 3, 1], [1])$, one has $r_1 = 3$ and:

$$\begin{array}{|c|c|c|} \hline & & \times \\ \hline & & \\ \hline & & \\ \hline \end{array} \rightarrow \begin{array}{|c|c|c|c|} \hline 1 & 1 & 1 & 4 \\ \hline 2 & 2 & 2 & \\ \hline 3 & & & \\ \hline \end{array} = S_1. \quad (14)$$

- For the second couple (β_{q_2}, l_2) , we let aside the vector l_2 for step 3, and we first create S_2^{hws} the highest weight state SSYT of shape β_{q_2} , and then we reindex the numbers in S_2^{hws} to get \tilde{S}_2^{hws} : $1 \rightarrow L$, $2 \rightarrow L - 1$, etc, where $L = r_1 + r_2 + 2$, where r_2 is the number of rows of β_{q_2} without the boxes containing the cross. Then, for our example, one has $(\beta_{q_2}, l_2) = ([4, 3, 2, 1], [32])$ and $r_2 = 4$, $L = 9$:

$$\begin{array}{|c|c|c|c|} \hline & & & \\ \hline & & \times & \\ \hline & \times & & \\ \hline & & & \\ \hline \end{array} \rightarrow \begin{array}{|c|c|c|c|} \hline 1 & 1 & 1 & 1 \\ \hline 2 & 2 & 2 & \\ \hline 3 & 3 & & \\ \hline 4 & & & \\ \hline \end{array} = S_2^{\text{hws}} \rightarrow \begin{array}{|c|c|c|c|} \hline 9 & 9 & 9 & 9 \\ \hline 8 & 8 & 8 & \\ \hline 7 & 7 & & \\ \hline 6 & & & \\ \hline \end{array} = \tilde{S}_2^{\text{hws}}. \quad (15)$$

Step 2

- We then expand the product $S_1 \otimes \tilde{S}_2^{\text{hws}}$ on the shape $\bar{\gamma}_L$ using the $U(r_1 + r_2 + 2) \supset U(r_1 + 1) \otimes U(r_2 + 1)$ subduction coefficients.⁶¹ One must find a linear superposition of SSYT's of shape $\bar{\gamma}_L$ having the same properties of "internal symmetries" between particles as the product $S_1 \otimes \tilde{S}_2^{\text{hws}}$. In particular, $S_1 \otimes \tilde{S}_2^{\text{hws}}$ should have its first $r_1 + 1$ entries like in S_1 , and must satisfy the **defining properties of the highest weight state** of the shape β_{q_2} but applied on the numbers L , $L - 1, \dots$ and $L - r_2 + 1$. Thus, as a basis set of our first expansion, we create all the SSYT's of shape $\bar{\gamma}_L$, starting like S_1 , and with L in the last $\beta_{q_2}(1)$ bottoms corners, with $L - 1$ in the following $\beta_{q_2}(2)$ bottom corners, etc \dots . In particular, no equal number should appear in the same column. Thus, for our example, one should expand $S_1 \otimes \tilde{S}_2^{\text{hws}}$ on the set:

$$\begin{array}{|c|c|c|c|} \hline 1 & 1 & 1 & 4 \\ \hline 2 & 2 & 2 & 8 \\ \hline 3 & 7 & 7 & 9 \\ \hline 6 & 8 & 8 & \\ \hline 9 & 9 & 9 & \\ \hline \end{array} \quad \begin{array}{|c|c|c|c|} \hline 1 & 1 & 1 & 4 \\ \hline 2 & 2 & 2 & 8 \\ \hline 3 & 6 & 7 & 9 \\ \hline 7 & 8 & 8 & \\ \hline 9 & 9 & 9 & \\ \hline \end{array} \quad \begin{array}{|c|c|c|c|} \hline 1 & 1 & 1 & 4 \\ \hline 2 & 2 & 2 & 7 \\ \hline 3 & 6 & 7 & 9 \\ \hline 8 & 8 & 8 & \\ \hline 9 & 9 & 9 & \\ \hline \end{array} \quad \begin{array}{|c|c|c|c|} \hline 1 & 1 & 1 & 4 \\ \hline 2 & 2 & 2 & 6 \\ \hline 3 & 7 & 7 & 9 \\ \hline 8 & 8 & 8 & \\ \hline 9 & 9 & 9 & \\ \hline \end{array} \quad (16)$$

The defining properties of \tilde{S}_2^{hws} imply that $S_1 \otimes \tilde{S}_2^{\text{hws}}$ should nullify the non negative operator $\text{Op}_{\bar{\gamma}_L}^{S_1 \otimes \tilde{S}_2^{\text{hws}}} = \sum_{q=0}^{k_2-2} E_{L-q-1, L-q} E_{L-q, L-q-1}$, where k_2 is the number of rows of β_{q_2} , i.e $k_2 = \text{Max}\{j \mid \beta_{q_2}(j) \neq 0\}$. Note that if there is just one row in β_{q_2} , then $k_2 = 1$, the set of SSYT for the expansion of $S_1 \otimes \tilde{S}_2^{\text{hws}}$ is reduced to only one SSYT, there is no term in $\text{Op}_{\bar{\gamma}_L}^{S_1 \otimes \tilde{S}_2^{\text{hws}}}$ and no need to build it. For our example, $\text{Op}_{\bar{\gamma}_L}^{S_1 \otimes \tilde{S}_2^{\text{hws}}}$ is represented, on the basis of Eq. 16, by the following matrix:

$$\begin{pmatrix} 2 & \sqrt{2} & 0 & 0 \\ \sqrt{2} & \frac{17}{5} & \frac{6}{5} & 0 \\ 0 & \frac{6}{5} & \frac{49}{15} & \frac{2\sqrt{2}}{3} \\ 0 & 0 & \frac{2\sqrt{2}}{3} & \frac{1}{3} \end{pmatrix}, \quad (17)$$

that we have calculated from the matrix elements of the generators $E_{L-q-1, L-q}$ using the Gelfand-Tsetlin rules⁸⁹ (cf the appendix of⁶³). By Gaussian elimination or by diagonalization, one obtains for $S_1 \otimes \tilde{S}_2^{\text{hws}}$:

$$\begin{array}{|c|c|c|c|} \hline 1 & 1 & 1 & 4 \\ \hline 2 & 2 & 2 & \\ \hline 3 & & & \\ \hline \end{array} \otimes \begin{array}{|c|c|c|c|} \hline 9 & 9 & 9 & 9 \\ \hline 8 & 8 & 8 & \\ \hline 7 & 7 & & \\ \hline 6 & & & \\ \hline \end{array} = \frac{-1}{5\sqrt{3}} \begin{array}{|c|c|c|c|} \hline 1 & 1 & 1 & 4 \\ \hline 2 & 2 & 2 & 8 \\ \hline 3 & 7 & 7 & 9 \\ \hline 6 & 8 & 8 & \\ \hline 9 & 9 & 9 & \\ \hline \end{array} + \frac{\sqrt{2}}{5\sqrt{3}} \begin{array}{|c|c|c|c|} \hline 1 & 1 & 1 & 4 \\ \hline 2 & 2 & 2 & 8 \\ \hline 3 & 6 & 7 & 9 \\ \hline 7 & 8 & 8 & \\ \hline 9 & 9 & 9 & \\ \hline \end{array} \\ - \frac{2\sqrt{2}}{5\sqrt{3}} \begin{array}{|c|c|c|c|} \hline 1 & 1 & 1 & 4 \\ \hline 2 & 2 & 2 & 7 \\ \hline 3 & 6 & 7 & 9 \\ \hline 8 & 8 & 8 & \\ \hline 9 & 9 & 9 & \\ \hline \end{array} + \frac{8}{5\sqrt{3}} \begin{array}{|c|c|c|c|} \hline 1 & 1 & 1 & 4 \\ \hline 2 & 2 & 2 & 6 \\ \hline 3 & 7 & 7 & 9 \\ \hline 8 & 8 & 8 & \\ \hline 9 & 9 & 9 & \\ \hline \end{array} \quad (18)$$

Note that in general, the dimension of the nullspace of $\text{Op}_{\bar{\gamma}_L}^{S_1 \otimes \tilde{S}_2^{\text{hws}}}$ is equal to the outer multiplicity of $\bar{\gamma}_L$ in $\beta_{q_1} \otimes \beta_{q_2}$, i.e $T_{N_s+1}^{\bar{\gamma}_L}(q_1, q_2)$. The coefficients in the right hand side (rhs) of Eq. 18 are some $U(r_1 + r_2 + 2) \supset U(r_1 + 1) \otimes U(r_2 + 1)$ subduction coefficients.

Step 3

We apply a linear superposition of product of hopping between consecutive sites $E_{q+1, q}$, to put the n_2 cross at the rows specified by the entries of the vector l_2 . We detail here how to obtain such a linear superposition on our example $(\beta_{q_2}, l_2) = ([4, 3, 2, 1], [32])$, in which there are $n_2 = 2$ cross. We proceed cross by cross from the one at the highest row, in order to transform

$$S_1 \otimes \tilde{S}_2^{\text{hws}} = \begin{array}{|c|c|c|c|} \hline 1 & 1 & 1 & 4 \\ \hline 2 & 2 & 2 & \\ \hline 3 & & & \\ \hline \end{array} \otimes \begin{array}{|c|c|c|c|} \hline 9 & 9 & 9 & 9 \\ \hline 8 & 8 & 8 & \\ \hline 7 & 7 & & \\ \hline 6 & & & \\ \hline \end{array} \quad (19)$$

into

$$S_1 \otimes \tilde{S}_2 = \begin{array}{|c|c|c|c|} \hline 1 & 1 & 1 & 4 \\ \hline 2 & 2 & 2 & \\ \hline 3 & & & \\ \hline \end{array} \otimes \begin{array}{|c|c|c|c|} \hline 9 & 9 & 9 & 9 \\ \hline 8 & 8 & 5 & \\ \hline 7 & 5 & & \\ \hline 6 & & & \\ \hline \end{array}. \quad (20)$$

Let's detail the sequence of computations: First, one should determine the coefficients $\eta(\sigma)$ in the operation

$$\mathcal{T}_{S_2^{\text{hws}}}^{S_2^{1/n_2}} = \sum_{\sigma} \eta(\sigma) \mathcal{P}_{\sigma} = \sum_{\sigma} \eta(\sigma) \prod_{k=l_2(\text{end})}^{r_2} E_{\sigma(k)+1, \sigma(k)}, \quad (21)$$

that will be such that $\mathcal{T}_{S_2^{\text{hws}}}^{S_2^{1/n_2}} S_2^{\text{hws}} = S_2^{1/n_2}$, which, for our example, reads:

$$S_2^{1/n_2} = \begin{array}{|c|c|c|c|} \hline 1 & 1 & 1 & 1 \\ \hline 2 & 2 & 5 & \\ \hline 3 & 3 & & \\ \hline 4 & & & \\ \hline \end{array}, \quad (22)$$

since the highest row for the first cross in $(\beta_{q_2}, l_2) = ([4, 3, 2, 1], [32])$ is row number $l_2(n_2) = l_2(\text{end}) = 2$. To determine the coefficients $\eta(\sigma)$ in Eq. 21, one could consider all the permutations σ of $\{l_2(\text{end}), l_2(\text{end}) + 1, \dots, r_2\} = \{2, 3, 4\}$, but for tall SSYT S_2^{hws} , with a cross located in the first rows, it won't be efficient, as we will handle a lot of permutations. Such a number of permutation is $(r_2 - l_2(\text{end}) +$

1)!, which is equal to $3! = 6$ in our example, but we will show that one can write $\mathcal{T}_{S_2^{\text{hws}}}^{S_2^{1/n_2}}$ as a sum of only four different terms. In fact, applied on the highest weight SSYT S_2^{hws} , each hopping term $E_{\sigma(k)+1, \sigma(k)}$ appearing in a product $\mathcal{P}_\sigma = \prod_{k=l_2(\text{end})}^{r_2} E_{\sigma(k)+1, \sigma(k)}$ will just change the numbers in the **edges** boxes (cf Fig. 8) between row $l_2(\text{end})$ and row r_2 , in such a way that the selection of the minimal set of permutations σ just requires the generation of the tree shown in Fig 8. At each stage of the tree, we just use the defining constraints of the SSYT for the edge boxes to know whether the product by a hopping term $E_{\sigma(k)+1, \sigma(k)}$ is possible whether it gives 0, and which new SSYT it can create. We then select the minimal number of permutations σ such that the products \mathcal{P}_σ can generate the largest number of different SSYT, which in particular, should contain $S_2^{1/n_2} = S_2^{1/2}$. Thus for our example, the four products of hopping terms are:

$$\begin{aligned} \mathcal{P}_{\sigma_1} &= E_{5,4}E_{4,3}E_{3,2} & \mathcal{P}_{\sigma_2} &= E_{3,2}E_{5,4}E_{4,3} \\ \mathcal{P}_{\sigma_3} &= E_{4,3}E_{3,2}E_{5,4} & \mathcal{P}_{\sigma_4} &= E_{3,2}E_{4,3}E_{5,4} \end{aligned} \quad (23)$$

Finally, we apply the Gelfand-Tsetlin rules^{63,89} to calculate all the $\mathcal{P}_\sigma S_2^{\text{hws}}$, and we obtain a linear system to get the coefficients $\eta(\sigma)$ such that Eq. 21 is satisfied. On our example, it gives:

$$\begin{aligned} \mathcal{P}_{\sigma_1} S_2^{\text{hws}} &= \sqrt{\frac{15}{8}}|A\rangle + \sqrt{\frac{3}{4}}|B\rangle + \sqrt{\frac{9}{8}}|C\rangle + \sqrt{\frac{1}{2}}|D\rangle, \\ \mathcal{P}_{\sigma_2} S_2^{\text{hws}} &= \sqrt{3}|B\rangle + |D\rangle, \\ \mathcal{P}_{\sigma_3} S_2^{\text{hws}} &= \sqrt{2}|C\rangle + |D\rangle, \\ \mathcal{P}_{\sigma_4} S_2^{\text{hws}} &= 2|D\rangle, \end{aligned} \quad \text{where}$$

$$|A\rangle = S_2^{1/n_2} = \begin{array}{|c|c|c|c|} \hline 1 & 1 & 1 & 1 \\ \hline 2 & 2 & 5 & \\ \hline 3 & 3 & & \\ \hline 4 & & & \\ \hline \end{array}, \quad |B\rangle = \begin{array}{|c|c|c|c|} \hline 1 & 1 & 1 & 1 \\ \hline 2 & 2 & 3 & \\ \hline 3 & 5 & & \\ \hline 4 & & & \\ \hline \end{array},$$

$$|C\rangle = \begin{array}{|c|c|c|c|} \hline 1 & 1 & 1 & 1 \\ \hline 2 & 2 & 4 & \\ \hline 3 & 3 & & \\ \hline 5 & & & \\ \hline \end{array}, \quad |D\rangle = \begin{array}{|c|c|c|c|} \hline 1 & 1 & 1 & 1 \\ \hline 2 & 2 & 3 & \\ \hline 3 & 4 & & \\ \hline 5 & & & \\ \hline \end{array}, \quad \text{so that} \quad (24)$$

$$\mathcal{T}_{S_2^{\text{hws}}}^{S_2^{1/n_2}} = \left\{ \sqrt{\frac{8}{15}}\mathcal{P}_{\sigma_1} - \sqrt{\frac{2}{15}}\mathcal{P}_{\sigma_2} - \sqrt{\frac{3}{10}}\mathcal{P}_{\sigma_3} + \sqrt{\frac{3}{40}}\mathcal{P}_{\sigma_4} \right\}.$$

In order to put the second cross at row number $l_2(n_2 - 1) (= l_2(1) = 3$ here), we first select the minimal number of relevant permutations within $\{l_2(1), l_2(1) + 1, \dots, r_2\} (= \{3, 4\})$, before solving the linear system to generate S_2^{2/n_2} from S_2^{1/n_2} , as:

$$\begin{aligned} S_2^{2/n_2} &= \begin{array}{|c|c|c|c|} \hline 1 & 1 & 1 & 1 \\ \hline 2 & 2 & 5 & \\ \hline 3 & 5 & & \\ \hline 4 & & & \\ \hline \end{array} = \mathcal{T}_{S_2^{1/n_2}}^{S_2^{2/n_2}} S_2^{1/n_2} \\ &= \left\{ \frac{2}{3}E_{5,4}E_{4,3} - \frac{1}{3}E_{4,3}E_{5,4} \right\} \begin{array}{|c|c|c|c|} \hline 1 & 1 & 1 & 1 \\ \hline 2 & 2 & 5 & \\ \hline 3 & 3 & & \\ \hline 4 & & & \\ \hline \end{array}. \end{aligned} \quad (25)$$

Cross by cross, we proceed the same way to determine all the coefficients in the operators $\mathcal{T}_{S_2^{k/n_2}}^{S_2^{k+1/n_2}}$, for $k =$

$0, 1, \dots, n_2 - 1$, with $S_2^{0/n_2} \equiv S_2^{\text{hws}}$, to build the product $R_{S_2^{\text{hws}}}^{S_2^{n_2/n_2}} = \mathcal{T}_{S_2^{n_2-1/n_2}}^{S_2^{n_2/n_2}} \dots \mathcal{T}_{S_2^{1/n_2}}^{S_2^{2/n_2}} \mathcal{T}_{S_2^{\text{hws}}}^{S_2^{1/n_2}}$. Then, we replace the numbers $1, 2, \dots, r_2 + 1$ by $L, L - 1, \dots, r_1 + 2$ in $R_{S_2^{\text{hws}}}^{S_2^{n_2/n_2}}$ to obtain $\tilde{R}_{S_2^{\text{hws}}}^{S_2^{n_2/n_2}}$ and we apply $\tilde{R}_{S_2^{\text{hws}}}^{S_2^{n_2/n_2}}$ on $S_1 \otimes \tilde{S}_2^{\text{hws}}$ to obtain $S_1 \otimes \tilde{S}_2$:

$$S_1 \otimes \tilde{S}_2 = \tilde{R}_{S_2^{\text{hws}}}^{S_2^{n_2/n_2}} S_1 \otimes \tilde{S}_2^{\text{hws}}, \quad (26)$$

where we use the expansion obtained at the end of step 2 for $S_1 \otimes S_2^{\text{chws}}$.

Step 4 & 5 & 6

We perform the steps 1 & 2 and 3 but with (β_{q_3}, l_3) instead of (β_{q_1}, l_1) and (β_{q_4}, l_4) instead of (β_{q_2}, l_2) .

Step 7

We finally use (again) the Gelfand-Tsetlin rules⁸⁹ (cf the appendix of⁶³) on the irrep $\bar{\gamma}_L$ seen as an irrep of the unitary group $U(L = r_1 + r_2 + 2)$ to calculate:

$$\begin{aligned} &\langle \beta_{q_3}, l_3 | \otimes \langle \beta_{q_4}, l_4 | E_{N_s+1, N_s+2}^{\bar{\gamma}_L} | \beta_{q_1}, l_1 \rangle \otimes | \beta_{q_2}, l_2 \rangle \\ &= \langle S_3 \otimes \tilde{S}_4 | E_{r_1+1, r_1+2} | S_1 \otimes \tilde{S}_2 \rangle. \end{aligned} \quad (27)$$

which is equal to $\sqrt{3/8}$ in our example.

The above method for the computation of the SU(N) symmetry-resolved reduced matrix elements of the interaction between the two blocks scales advantageously with N , as compared with others methods based on the Wigner 9j or 6j coefficients or on related coefficients (like the X symbols⁹⁸) which naturally arise through the Wigner-Eckart theorem (cf Eq. (8) in⁹⁹ and Eq. (32) in¹⁰⁰). The reason is that, apart from SU(2) where there are closed-form expression (cf Eq. (3.326) in¹⁰¹), the calculation of SU(N) Wigner n-j (n=6 or 9) coefficients^{102,103} is most frequently based on summation over Clebsch-Gordan coefficients, whose time of computation is a polynomial (cf section XII in⁷⁰) in the dimensions of the two SU(N) irreps $\bar{\beta}_{q_1}^T$ and $\bar{\beta}_{q_2}^T$ (or $\bar{\beta}_{q_3}^T$ and $\bar{\beta}_{q_4}^T$), which are the SU(N) Young diagrams before transposition. In the example above, the SU(4) irrep $\bar{\beta}_{q_1}^T = [3221]$ (resp. $\bar{\beta}_{q_2}^T = [4321]$) has dimension 15 (resp. 64), so that we can still survive with Clebsch-Gordan based methods, however, we are able to calculate:

$$\begin{aligned} &\langle \beta_{q_3}, l_3 | \otimes \langle \beta_{q_4}, l_4 | E_{N_s+1, N_s+2}^{\bar{\gamma}_L} | \beta_{q_1}, l_1 \rangle \otimes | \beta_{q_2}, l_2 \rangle = \sqrt{\frac{32}{27}}, \\ &\text{with} \quad \bar{\gamma}_L = [66666662], \\ &\beta_{q_1}, l_1 = [654321], [51] \quad \beta_{q_2}, l_2 = [6543221], [641], \\ &\beta_{q_3}, l_3 = [654421], [541] \quad \beta_{q_4}, l_4 = [6542221], [61], \end{aligned} \quad (28)$$

in few seconds on a laptop. In particular the dimension of $\text{Op}_{\bar{\gamma}_L}^{S_1 \otimes S_2^{\text{hws}}}$, which gives the number of terms in the linear superposition at the end of step 2 (cf. Eqs. (16) and (18)) is 164. This is much smaller than the dimension of the SU(6) irreps $\beta_{q_1}^T = [654321]$ and $\beta_{q_2}^T = [764321]$, which are respectively 32768 and 145530, which are way too large to allow us for the computation of the above reduced matrix element with summation over Clebsch-Gordan coefficients.

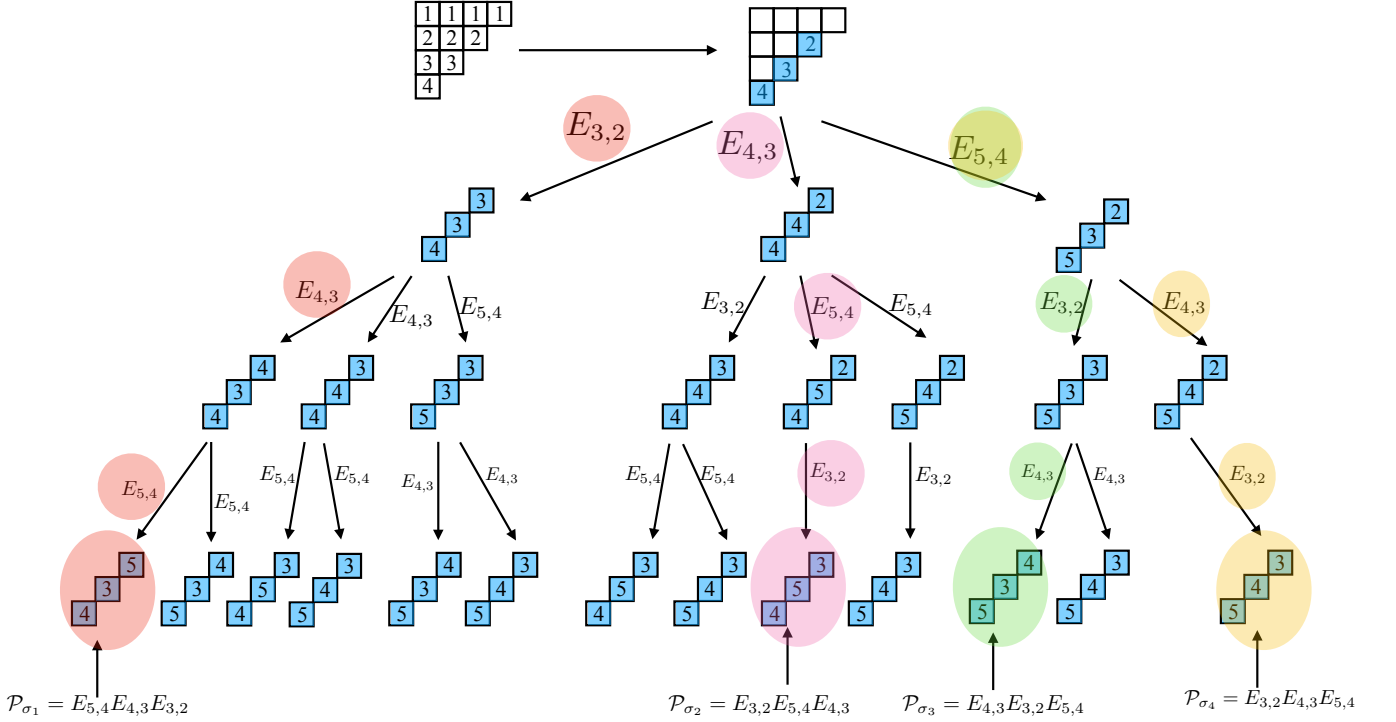


FIG. 8. Example of tree generated by the application of operators of the form $\mathcal{P}_\sigma = \prod_{k=l_2(\text{end})}^{r_2} E_{\sigma(k)+1, \sigma(k)}$ for $\beta_{q_2} = [432]$, $l_2(\text{end}) = 2$ and $r_2 = 4$, where σ is a permutation of $\{l_2(\text{end}), l_2(\text{end}) + 1, \dots, r_2\} = \{2, 3, 4\}$ (cf text for details). From this tree, our purpose is to select the minimal set of permutations $\{\sigma\}$ to generate the largest variety of SSYT (containing S_2^{1/n_2} , cf Eq. 22) appearing on the last line of the tree. In particular, each time an operator $E_{\sigma(k)+1, \sigma(k)}$ acts on a SSYT, either it vanishes, either it creates some SSYTs where one number in the **edge boxes** has changed. On a given SSYT, for each row between row $l_2(\text{end}) = 2$ and row $r_2 = 4$ inclusive, the edge boxes are the rightmost boxes and appear in blue in the figure.

Finally, let's mention the changes implied by outer multiplicity $T_{N_s+1}^{\tilde{\gamma}_L}(q_1, q_2) > 1$. $T_{N_s+1}^{\tilde{\gamma}_L}(q_1, q_2)$ is the dimension of the nullspace of $\text{Op}_{\tilde{\gamma}_L}^{S_1 \otimes S_2^{\text{hws}}}$, so that there is a freedom (gauge) in the $T_{N_s+1}^{\tilde{\gamma}_L}(q_1, q_2)$ vectors of subduction coefficients in the rhs of Eq. 18 defining the basis of such a nullspace¹⁰⁴. One then requires some consistency in the selection of the basis: the way the coefficients are chosen is fixed for a given set of irreps $\tilde{\gamma}_L, \beta_{q_1}$ and β_{q_2} , and one introduces an additional index $k_i = 1, 2, \dots, T_{N_s+1}^{\tilde{\gamma}_L}(q_1, q_2)$, to refer to the k_i^{th} basis state of such a nullspace, which should be added in both the bra and the ket of reduced matrix elements in Eq. 12. Steps 3 and steps 7 are kept identical.

III. DMRG RESULTS FOR THE SU(N) FERMI-HUBBARD CHAIN WITH OPEN BOUNDARY CONDITIONS

As an application of our DMRG algorithm, we have numerically investigated the Metal-Insulator transition in the one-dimensional SU(N) FHM with OBC for $N = 3, 4$ and $N = 6$ at filling $1/N$. We set the hopping amplitude $t \equiv 1$ in the following, and plot the energies and gaps as a function of the coupling U . Our purpose was to confirm numerically some field theory predictions made in the paper.⁹⁰ In particular, we

want at first to calculate the critical value of U at the transition (that we call U_c) as a function of N , and secondly to characterize the effective critical low energy theories in both the metallic and the insulating phases by calculating the central charges. Note that other numerical works already focused on this model, as summarized in,^{31,32} and we will compare some of their results to ours, but let's mention before that we were able to address either larger system sizes (typically $L \sim 100$ before extrapolation), either larger N than in previous works.

As opposed to $N = 2$, where the phase is insulating as soon as $U > 0$ (like for the square lattice), for $N > 2$, it is expected⁹⁰ to have a Kosterlitz-Thouless (KT) transition at finite $U_c > 0$, with a charge gap Δ_c behaving (in the thermodynamical limit) as:

$$\Delta_c = C_{KT} \exp\left(-\frac{G_{KT}}{\sqrt{U - U_c}}\right), \quad (29)$$

for $U > U_c$ and zero otherwise.

The (finite-size) charge gap is defined as:

$$\Delta_c = \sum_{\epsilon=\pm 1} E_0(f_L = \frac{L+\epsilon}{NL}) - 2E_0(f_L = \frac{1}{N}), \quad (30)$$

where $E_0(f_L)$ is the minimal energy for the L -sites chain with filling f_L . In particular, $f_L = \frac{1}{N}$ means that there is one

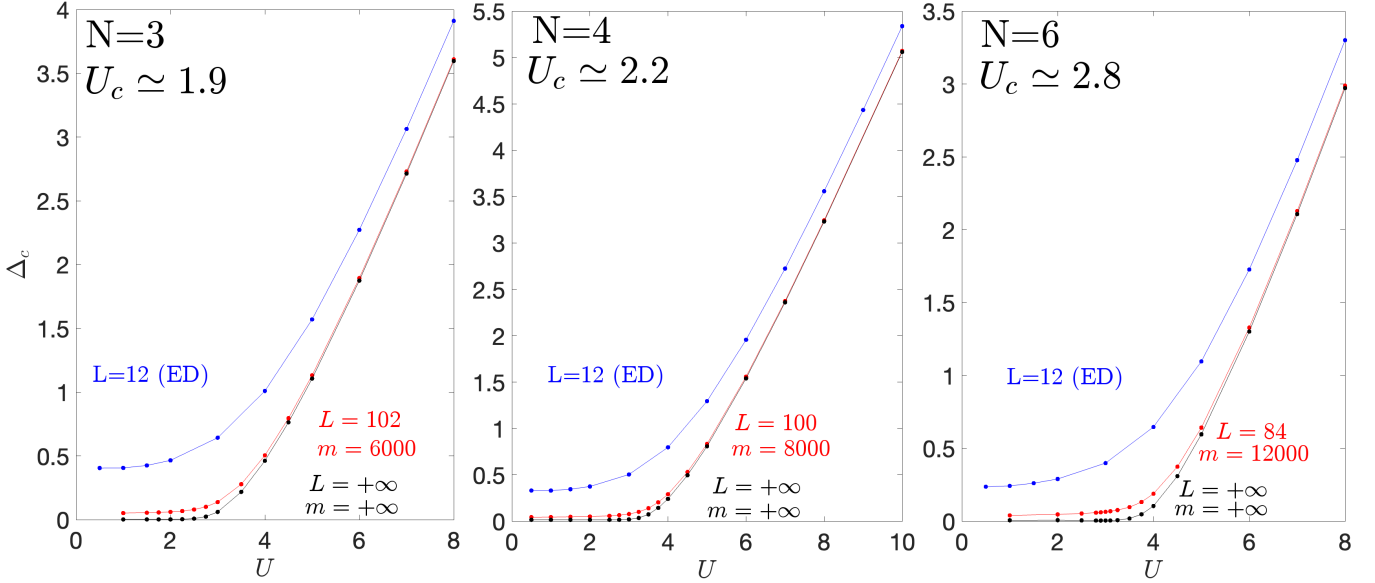


FIG. 9. Charge gaps Δ_c for $N = 3$ (left), $N = 4$ (middle), and $N = 6$ (right), as a function of U . We calculated the ground state energies E_0 of the Hamiltonian in Eq. 3 for $t = 1$ as a function of U , for the three doping $\delta = 0, \pm 1$, (i.e or fillings $f_L = 1/N + \delta/(NL)$) corresponding to three different targeted irreps (cf Eq. 30 for the definition of Δ_c). For $L = 12$ (in blue), we used ED, while for $L = L_{\text{Max}}^{\Delta_c} = 102$ ($N = 3$), 100 ($N = 4$) and 84 ($N = 6$), we used our DMRG algorithm with full $SU(N)$ symmetry with $m = 6000$ ($N = 3$), $m = 8000$ ($N = 4$) and $m = 12000$ states kept ($N = 6$) (cf also Tab. II for some numerical values). In black, extrapolated values (cf Fig. 10 for the extrapolation procedure) in the limit $L \rightarrow +\infty, m \rightarrow +\infty$. See text for details.

particle per site on average, while $f_L = \frac{L+1}{NL}$ (resp. $f_L = \frac{L-1}{NL}$) means one particle (resp. hole) away from the filling $1/N$. Introducing the doping $\delta = 0, \pm 1$, the total number of particles reduces to $f_L NL = L + \delta$. Note that the quantity Δ_c , presented in Eq. 30 as the definition of the charge gap in accordance with,⁹⁰ can instead be interpreted as the finite-size compressibility. Regardless of the terminology, however, this quantity serves in any case as an indicator of the metal-insulator transition.

From ED on small chains, we were able to scrutinize all the relevant irreps for the three different doping δ (or fillings f_L), and to infer that the ground state for $U \geq 0.5$ should always live in the most antisymmetric N -rows and $f_L NL$ -boxes YD, which will be the targeted shape γ_L (before transposition). We have also used the ED ground state energies E_0 and charge gap Δ_c for $L = 12$ to benchmark our code, and we show these quantities for $N = 2, 3, 4$ and 6, for filling $1/N$ and for $U = 1$ and $U = 5$ in Tab. I. For $N = 3$, $m = 8000$ states kept and $M = 300$ irreps, we have 10 (resp. 9) good digits for E_0 at $U = 5$ (resp. $U = 1$), while for $N = 6$, $m = 12000$ states kept and $M = 420$ irreps, we have 7 (resp. 6) good digits at $U = 5$ (resp. $U = 1$). It is a general trend that we have observed in all our simulations: as we will show below, for all values of N , $U = 5$ (resp. $U = 1$) will be in the insulating (resp. metallic) phase, and the numerical convergence is better in the insulating phase than in the metallic phase, due to the Casimir-based truncation of the M irreps (cf Fig. 3 a).

For each value of N and U that we have considered, we have performed the infinite size DMRG up to $L = L_{\text{Max}}^{\Delta_c}$ for

N	$E_0(U = 1)$	$\Delta_c(U = 1)$	$E_0(U = 5)$	$\Delta_c(U = 5)$
2	-11.840637285901	0.53823	-5.535630158601	2.42139
3	-15.376173634063	0.40623	-7.024399312653	1.57037
4	-16.722033360620	0.33088	-7.602319080277	1.29482
6	-17.700163882249	0.24275	-8.029094742355	1.09706

TABLE I. Exact Ground state Energies E_0 (at filling $1/N$, i.e doping $\delta = 0$) and charge gap Δ_c (cf Eq. 30) of the $SU(N)$ FHM on the chain with OBC for $L=12$ sites calculated through Exact Diagonalization for $U = 1$ and $U = 5$. We have exactly diagonalized the Hamiltonian shown in Eq. 3 (from which we have withdrawn the constant $-LU/2$ for convenience) taking into account the full $SU(N)$ symmetry using the method introduced in.⁶³

the three different filling $f_L NL = L + \delta$ ($\delta = 0, \pm 1$), and for several (at least two) values of m , i.e. the number of states kept, and (unless otherwise specified) for $M = 300$ irreps kept. For instance, for $N = 4$, $L_{\text{Max}}^{\Delta_c} = 100$, we made simulations with $m = 6000, 8000$ and 10000. We show in Tab. II, some DMRG results for the total ground state Energy $E_0(m, L)$ and discarded weight $\mathcal{W}_d^{m, L}$ at doping $\delta = 0$, for various values of N and L as well as the charge gaps $\Delta_c(m, L)$ obtained from the three simulations (i.e $f_L = (1/N) + \delta/(NL)$ with $\delta = 0, \pm 1$, cf Eq. 30), for $U = 1$ and $U = 5$. This latter quantity is also plotted in red as a function of U in Fig. 9. We also made two different kinds of extrapolation. A first extrapolation gives our best estimate of the minimal energies at fixed L . It is made by using the loss weight $\mathcal{W}_d^{m, L}$ (in the abscissa) obtained for

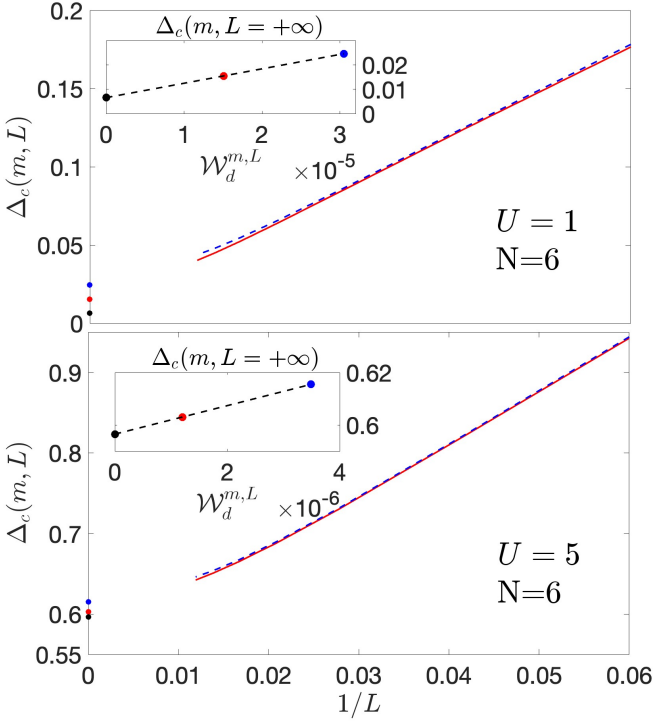


FIG. 10. Charge gaps $\Delta_c(m, L)$ for $N=6$ for $m = m_2 = 12000$ (resp. $m = m_1 = 8000$) states kept in solid red (resp. dashed blue) lines, for $U = 1$ (top) and $U = 5$ (bottom) as a function of $1/L$. At fixed m , we extrapolate the gaps in the thermodynamical limit $L \rightarrow \infty$, fitting the points $\Delta_c(m, L)$ with a function of the form $a + b/L + d/L^2$ to obtain $\Delta_c(m, L = +\infty) = a$, shown as colored points on the y axis. Insets: values $\Delta_c(m, L = +\infty)$ plotted as a function of the discarded weight $\mathcal{W}_d^{m, L}$ for $L = L_{\text{Max}}^{\Delta_c} = 84$. We make a linear extrapolation $\mathcal{W}_d^{m, L}$ to obtain $\Delta_c(m = +\infty, L = +\infty)$ in black, which is tabulated in Tab. II and plotted as a function of U in Fig. 9.

various values of m : in the limit $m \rightarrow +\infty$, $\mathcal{W}_d^{m, L} \rightarrow 0$, and $E_0(m, L) \rightarrow E_0(m = +\infty, L)$, where $E_0(m = +\infty, L)$ is obtained through a linear fitting. $E_0(m = +\infty, L)$ for $L = 36, 48$ and 84 and for $U = 1$ and 5 and the largest values of m used for the extrapolation (i.e. m_{Max}) are shown in Tab. II.

A second extrapolation is made at fixed m in the thermodynamical limit $L \rightarrow \infty$, fitting the points $\Delta_c(m, L)$ with a function of the form $a + b/L + d/L^2$ to obtain $\Delta_c(m, L = +\infty) = a$, as illustrated in Fig. 10, for $N = 6$.

Then, we take the limit $m \rightarrow +\infty$ in $\Delta_c(m, L = +\infty)$, using the first kind of extrapolation, i.e with the discarded weight at $L = L_{\text{Max}}^{\Delta_c}$, as shown in the insets of Fig. 10), to get $\Delta_c(m = +\infty, L = +\infty)$ ¹⁰⁵. To make this extrapolation for many values of U , we considered simulations with m_1 and m_2 states kept, where m_1 and m_2 are tabulated in Tab. II. We show the resulting $\Delta_c(m = +\infty, L = +\infty)$ in black as a function of U in Fig. 9. We fit $\Delta_c(m = +\infty, L = +\infty)$ with the function shown in Eq. 29 to obtain our estimates of U_c

which read (cf also Fig. 9):

$$\begin{aligned} U_c(N = 3) &\simeq 1.9, \\ U_c(N = 4) &\simeq 2.2, \\ U_c(N = 6) &\simeq 2.8. \end{aligned} \quad (31)$$

In spite of the good accuracy of our DMRG energies (error of the order of the discarded weight $\sim 1e-5$ at worst, depending on N , $L_{\text{Max}}^{\Delta_c}$ and δ , cf also Tab. II), obtaining these values for U_c with error bar ~ 0.1 was a complicated task: even for $U = U_c + 0.5$, the (expected or fitted) gap Δ_c is still very small due to the exponential function in Eq. 29. Note that for $N = 3$ and $N = 4$, our proposed values of U_c lie in between the ones calculated through Green's function Monte-Carlo in,⁹⁰ which read $U_c(N = 3) \simeq 2.2$ and $U_c(N = 4) \simeq 2.8$ and the ones calculated in¹⁰⁶ which are $U_c(N = 3) \simeq 1.1$ and $U_c(N = 4) \simeq 2.1$. These latter values were not calculated directly from the charge gaps but rather indirectly, from the fidelity susceptibility of the ground states as a function of U . Our finite values of U_c shown in Eq. 31, are also in contrast with the numerical results obtained in,¹⁰⁷ which argued for an opening of the gap for infinitesimal $U \forall N$, and not only for $N=2$.

Moreover, from the infinite DMRG part, we have also calculated the ground state energy per site $e_0(m, L)$ approximated as $e_0(m, L) = (E_0(m, L) - E_0(m, L - 2N))/(2N)$ and extrapolated at finite L in the limit $m \rightarrow +\infty$ using the discarded weight $\mathcal{W}_d^{m, L}$ (cf above), and in the thermodynamical limit $L \rightarrow +\infty$ through a quadratic fitting in $1/L$, to obtain $e_0(m = +\infty, L = +\infty)$ shown in Tab. II.

After the infinite size DMRG part, and once the desired length of the chain L , was reached, we have also performed some sweeps from left to right and from right to left through the finite-size DMRG. It involves the very same steps as in the infinite part, except that the left and the right blocks have now different sizes. In particular, the calculation of the matrix elements of the interaction term between the two blocks will depend on the $U(L) \subset U(x) \otimes U(L - x)$ subduction coefficients, where x is the length of the left block, which are computed using the very same method as before. For fixed m , we have computed the entanglement entropy $S(x)$ (cf Eq. (11)) as a function of x , the position of the sweep. For critical spin chains with OBC, the entanglement entropy is given by the Calabrese-Cardy formula:¹⁰⁸

$$S(x) = \frac{c}{6} \log \left[\frac{2L}{\pi} \sin \left(\frac{\pi x}{L} \right) \right] + K, \quad (32)$$

where K is a non-universal constant, and c is the central charge of the associated CFT.

For critical systems, c gives the number of critical modes for the effective low energy field theory. According to the bosonization approach developed in,⁹⁰ it should be here equal to $c_{\text{th}} = N$ for $U < U_c$ and $c_{\text{th}} = N - 1$ for $U > U_c$. In particular, the spin degrees of freedom are described by the $SU(N)_1$ WZW CFT^{19,81} with $N - 1$ gapless critical modes for arbitrary U , while the charge degrees of freedom are described by a sine-Gordon model, which becomes critical when $U < U_c$, adding another critical mode,

	U=1, N=3	U=5, N=3	U=1, N=4	U=5, N=4	U=1, N=6	U=5, N=6
m_{Max}	8000	8000	10000	10000	16000	12000
$E_0(m_{\text{Max}}, L = 36)$	-47.8504524	-21.9643200	-52.030618	-23.862852	-55.08724	-25.319341
$\mathcal{W}_d^{m_{\text{Max}}, L=36}$	7.5×10^{-10}	2.8×10^{-12}	6.5×10^{-8}	1.4×10^{-9}	1.1×10^{-6}	1.8×10^{-7}
$E_0(m = +\infty, L = 36)$	-47.8504525	-21.9643200	-52.030621	-23.862852	-55.08726	-25.319345
$E_0(m_{\text{Max}}, L = 60)$	-80.347158	-36.9109353	-87.35688	-40.131088	-92.4828	-42.61863
$\mathcal{W}_d^{m_{\text{Max}}, L=60}$	2.0×10^{-8}	4.9×10^{-11}	7.6×10^{-7}	1.4×10^{-8}	8.6×10^{-6}	1.3×10^{-6}
$E_0(m = +\infty, L = 60)$	-80.347160	-36.9109353	-87.35691	-40.131089	-92.4831	-42.61867
$E_0(m_{\text{Max}}, L = 84)$	-112.847267	-51.8586464	-122.68571	-56.400596	-129.8790	-59.91933
$\mathcal{W}_d^{m_{\text{Max}}, L=84}$	9.2×10^{-8}	2.3×10^{-10}	2.2×10^{-6}	4.8×10^{-8}	1.9×10^{-5}	2.7×10^{-6}
$E_0(m = +\infty, L = 84)$	-112.847276	-51.8586465	-122.68585	-56.400600	-129.8804	-59.91947
$e_0(m = +\infty, L = +\infty)$	-1.35428	-0.622858	-1.47213	-0.677939	-1.55829	-0.72092
$L_{\text{Max}}^{\Delta_c}$	102	102	100	100	84	84
m_1, m_2	4000,6000	4000,6000	6000,8000	6000,8000	8000,12000	8000,12000
$\Delta_c(m_2, L = L_{\text{Max}}^{\Delta_c})$	0.052	1.13	0.045	0.83	0.040	0.642
$\Delta_c(m = +\infty, L = +\infty)$	0.0022	1.11	0.016	0.81	0.0065	0.596
$c(m = m_{\text{Max}}, L = 48)$	2.51 2.77 3.11	1.48 1.66 2.03	3.30 3.66 4.10	2.15 2.48 2.90	5.11 5.49 6.55	4.30 4.66 5.82
$c(m = m_{\text{Max}}, L = 84)$	2.69 2.84 3.04	1.63 1.75 2.01	3.50 3.70 3.89	2.41 2.60 2.84	5.07 5.55 5.83	4.38 4.84 5.28

TABLE II. Finite-size and finite-m total ground state energies $E_0(m, L)$, discarded weight $\mathcal{W}_d^{m,L}$, charge gaps $\Delta_c(m, L)$, central charges $c(m, L)$ and extrapolated gaps $\Delta_c(m = +\infty, L = +\infty)$, ground state total energies $E_0(m = +\infty, L)$ and energies per site $e_0(m = +\infty, L = +\infty)$ of the SU(N) FHM on the chain with OBC for $L=36, 48, 84$ and $L = +\infty$ sites calculated through DMRG simulations with the full SU(N) symmetry, for $N = 3, 4$ and 6 , filling $1/N$ and for $U = 1$ and $U = 5$. The number of states kept $m = m_1, m_2$ and $m = m_{\text{Max}}$ and the maximal number of sites $L = L_{\text{Max}}^{\Delta_c}$ used for the extrapolation are also shown. For the energies, the constant $-LU/2$ was withdrawn for convenience. For the central charges, we give the three (ordered in ascending order) values $c_{\text{Floor}(N/2)}, \tilde{c}$ and c_0 , introduced in the text to take into account the Friedel oscillations in the fitting of the entanglement entropy $S(x)$ through the Calabrese-Cardy formula (cf Eq. 32). See text for additional details.

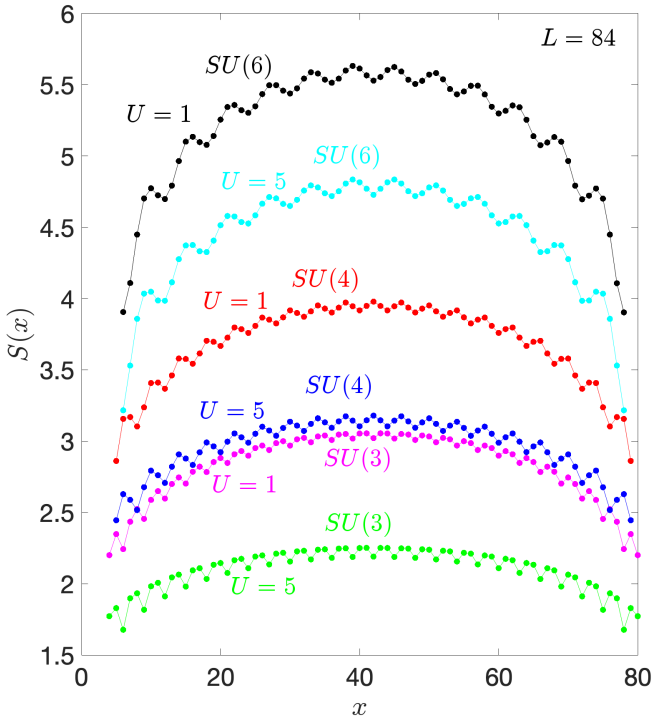


FIG. 11. Entanglement entropy $S(x)$ as a function of the position x along an open chain of $L = 84$ sites for $N = 3, 4, 6$ and $U = 1, 5$ at filling $1/N$. The number of states kept for each curve is m_{Max} shown in Tab. II. Due to the Open Boundary Conditions (OBC), the curves exhibit some Friedel oscillations which are N -periodic since the filling is $1/N$.

so that $c_{\text{th}} = N - \Theta(U - U_c)$, where Θ is the Heaviside step function. To characterize the two different critical phases, we show in Fig. 11 the profile of the entanglement entropy $S(x)$ as a function of the position x for $L = 84$, for $U = 1$, i.e. in the metallic phase, and for $U = 5$, i.e. in the insulating phase for all the values of N considered here, i.e. $N = 3, 4$ and 6 .

Because of the OBC and of the $1/N$ filling, $S(x)$ has Friedel oscillations with N -fold periodicity, that we should remove to fit the central charges. We adopt the very same strategy as in:⁶⁷ since the oscillations are N -periodic, one can plot $S(x)$ as a function of the logarithm of the conformal distance $\frac{1}{6} \log \left[\frac{2L}{\pi} \sin \left(\frac{\pi x}{L} \right) \right]$ separately for different sets of abscissa x of the form $x = N \times p + q$.

Each set corresponds to a fixed $q = 0, 1, \dots, N-1$ and to all values of p consistent with the overall length. As shown in Fig. 12, it then gives rise to several different straight lines (at most N , i.e. one for each q , not shown), with different slopes c_q . It turns out that one always has $\text{Min}(c_{\text{Floor}(N/2)}, c_0) \leq \dots \leq \text{Max}(c_{\text{Floor}(N/2)}, c_0)$, so that $c_{\text{Floor}(N/2)}$ and c_0 can be considered as the boundary values of the central charges.

Alternatively, one can also follow the strategy introduced in¹⁰⁹ and developed in:¹¹⁰ Since the Friedel oscillations originate from the bond modulations, it is convenient to introduce $\tilde{S}_k(x) = S(x) + k \langle E_{x,x+1} + \text{h.c.} \rangle$, where $\langle E_{x,x+1} \rangle$ is the expectation value on the ground state of the hopping between

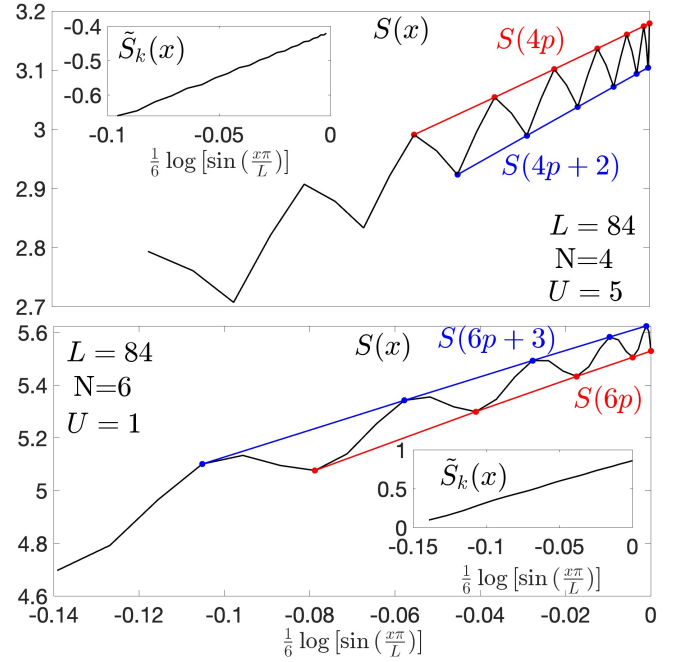


FIG. 12. Entanglement entropy $S(x)$ as a function of the logarithm of the conformal distance $\frac{1}{6} \log \left[\sin \left(\frac{\pi x}{L} \right) \right]$ shown for an open chain of $L = 84$ sites for $N=4$, $U = 5$ and $m = 10000$ states kept in the top figure, and for $N=6$, $U = 1$ and $m = 16000$ in the bottom figure. The position x is $x = N \times p + q$ (with $q = 0, 1, 2, \dots, N-1$), giving rise to a most N different straight lines. We show in red $q = 0$ and in blue $q = N/2$. Insets: we alternatively consider $\tilde{S}_k(x) = S(x) + k \langle E_{x,x+1} + \text{h.c.} \rangle$, with the best k to remove the Friedel oscillations, Here, $k = 2.842$ for $N=4$ and $k = 2.505$ for $N=6$. The three values $c_{\text{Floor}(N/2)}$, \tilde{c} and c_0 , are tabulated in Tab. II, and agree with the field theory predictions (cf text for details).

the left and the right block, and where k is a parameter that is adjusted to best remove the oscillations. From the fitting of $\tilde{S}_k(x)$ with the logarithm of the conformal distance, we extract \tilde{c} (cf Fig. 12) and we have systematically observed that $\text{Min}(c_{\text{Floor}(N/2)}, c_0) \leq \tilde{c} \leq \text{Max}(c_{\text{Floor}(N/2)}, c_0)$.

We show in Tab. II, these quantities for $L = 48$ and $L = 84$, and it exhibits good agreement with the field theory expectations, and suggest good evolution with the system sizes: $\tilde{c}(L = 48) \leq \tilde{c}(L = 84) \rightarrow c_{\text{th}}$ and the range given by $|c_0 - c_{\text{Floor}(N/2)}|$ also contracts. Like for the energies, the convergence of the entanglement entropy is easier in the Mott phase; actually the central charges were already observed to be close to $N - 1$ in previous studies, either for the pure Heisenberg $SU(N)$ models,^{67,111} either in the $SU(N)$ FHM for large U , (i.e. $U = 10t$ in¹¹²), although on smaller chains. Finally, the form of the finite-size corrections to the central charges, which, for $SU(2)$, is positive and scales as $1/\log(L)^3$ for PBC^{82,113} and is negative and scales as $1/\log(L)^2$ for OBC,^{114,115} is beyond the scope of our manuscript and would deserve further investigations.

IV. CONCLUSIONS AND PERSPECTIVES

To conclude, we have shown how to implement the full $SU(N)$ symmetry in a DMRG code "à la White" for the $SU(N)$ FHM using the basis of SSYT. In particular, we provided many details on the calculation of the hopping between the left and the right block, for which the subduction coefficients of the unitary groups play a key role, enabling us to bypass the calculation and the storage of the Clebsch-Gordan coefficients. Such a methodology becomes more and more advantageous as N increases (as shown at the end of the section [II C 1](#)). It renders possible the DMRG simulations of the $SU(N)$ FHM on the one dimensional chain at filling $1/N + \delta/NL$, ($\delta = 0, \pm 1$), up to $N = 6$ and $L = 84$ (before extrapolation) with a discarded weight $\mathcal{W}_d^{m,L}$ low enough to get 5 to 6 digits ground state energies. As an application, we computed U_c for the Metal-Insulator transition, and we have demonstrated that it is finite for $N > 2$, in contrast with some previous DMRG works, not implementing the full $SU(N)$ symmetry.¹⁰⁷ Thus, the implementation of non-Abelian symmetries is not merely aimed at slightly refining a numerical result but can also help solve a physical problem and settle a controversy. We have also calculated the central charges in both the metallic and the insulating phase, confirming the analytical quantum field theory predictions. In particular, our numerical results corroborate the presence of $N - \Theta(U - U_c)$, (where Θ is the Heaviside step function) gapless critical modes, endorsing the spin-charge separation picture elaborated from the bosonization approach.⁹⁰ $N - 1$ critical modes in the spin sector for every positive U , with an additional critical mode in the gap sector when the charge gap vanishes (i.e when $U < U_c$, in the metallic phase). Our simulations also provide us with accurate ED or DMRG ground state energy values for different parameters, which might be useful for benchmarking future numerical works.

As obvious perspectives, one could first think of addressing different boundary conditions (like the PBC), different fillings,^{45,57,58,107,112,116,117} other quasi one-dimensional ge-

ometries like the ladder,^{118–120} or models with longer range¹²¹ or non-uniform hopping, like the modulated $SU(N)$ FHM.¹²²

As a methodological outlook, a useful work would be the extension of the use of the subduction coefficients for the unitary group to other $SU(N)$ symmetry-resolved algorithms based on matrix product states (MPS) and to other kind of tensor networks which are available through on-line libraries,^{123–126} which are not always adapted to large N , as they are based on the calculation/storage/manipulation of Clebsch-Gordan coefficients which become computationally prohibitive when $N \geq 6$.

An other important direction of study would be the attempt to implement the $SU(N)$ symmetry in the numerical simulation of the multi-orbital FHM.^{30,127,128} In fact, the multi-orbital $SU(N)$ FHM can be regarded as an experimentally feasible class of models that, in the asymptotic limit of large on-site interactions, reduce to $SU(N)$ Heisenberg models with multi-column irreducible representations at each site.^{74,76,85,97,128–135} These spin models have recently attracted significant theoretical interest, as they may host various exotic one-dimensional phases, such as symmetry-protected topological phases.^{42–44,46,48,128,136} Realizing these models experimentally with cold atoms would require investigating their practically implementable counterpart: the multi-orbital $SU(N)$ FHM.

Finally, our algebraic approach based on the representations of the unitary group could also be used to study two-dimensional $SU(N)$ FHM which could potentially host $SU(N)$ chiral spin liquids.^{35,38,40,41}

Work is currently in progress along these lines.

V. ACKNOWLEDGEMENTS

We acknowledge useful discussions with Profs. P. Lecheminant and S. Capponi, and we thank the IT Systems Engineers J. Michel and J-D. Dubois for their instrumental assistance. The author is supported by the IRP EXQMS project from CNRS.

¹ T. Esslinger, Annual Review of Condensed Matter Physics **1**, 129 (2010), arXiv:1007.0012 [cond-mat.quant-gas].

² A. Mazurenko, C. S. Chiu, G. Ji, M. F. Parsons, M. Kanász-Nagy, R. Schmidt, F. Grusdt, E. Demler, D. Greif, and M. Greiner, Nature **545**, 462 (2017).

³ F. Schäfer, T. Fukuhara, S. Sugawa, Y. Takasu, and Y. Takahashi, Nature Reviews Physics **2**, 411 (2020).

⁴ S. Taie, R. Yamazaki, S. Sugawa, and Y. Takahashi, Nat Phys **8**, 825 (2012).

⁵ G. Pagano, M. Mancini, G. Cappellini, P. Lombardi, F. Schäfer, H. Hu, X.-J. Liu, J. Catani, C. Sias, M. Inguscio, and L. Fallani, Nature Physics **10**, 198 (2014).

⁶ F. Scazza, C. Hofrichter, M. Höfer, P. C. De Groot, I. Bloch, and S. Fölling, Nature Physics **10**, 779 (2014).

⁷ X. Zhang, M. Bishof, S. L. Bromley, C. V. Kraus, M. S. Safronova, P. Zoller, a. M. Rey, and J. Ye, Science (New York, N.Y.) **345**, 1467 (2014).

⁸ C. Hofrichter, L. Riegger, F. Scazza, M. Höfer, D. R. Fernandes, I. Bloch, and S. Fölling, Phys. Rev. X **6**, 021030 (2016).

⁹ B. Abeln, K. Sponselee, M. Diem, N. Pintul, K. Sengstock, and C. Becker, Phys. Rev. A **103**, 033315 (2021).

¹⁰ S. Taie, E. Ibarra-García-Padilla, N. Nishizawa, Y. Takasu, Y. Kuno, H.-T. Wei, R. T. Scalettar, K. R. A. Hazzard, and Y. Takahashi, Nature Physics **18**, 1356 (2022).

¹¹ D. Tusi, L. Franchi, L. F. Livi, K. Baumann, D. Benedicto Orenes, L. Del Re, R. E. Barfknecht, T. W. Zhou, M. Inguscio, G. Cappellini, M. Capone, J. Catani, and L. Fallani, Nature Physics **18**, 1201 (2022).

¹² G. Pasqualetti, O. Bettermann, N. Darkwah Oppong, E. Ibarra-García-Padilla, S. Dasgupta, R. T. Scalettar, K. R. A. Hazzard, I. Bloch, and S. Fölling, Phys. Rev. Lett. **132**, 083401 (2024).

¹³ J. Hubbard, Proc. R. Soc. London A - Math. Phys. Sci. **276**, 238 (1963).

¹⁴ M. C. Gutzwiller, Phys. Rev. Lett. **10**, 159 (1963).

- ¹⁵ D. J. Scalapino, *Rev. Mod. Phys.* **84**, 1383 (2012).
- ¹⁶ D. P. Arovas, E. Berg, S. A. Kivelson, and S. Raghu, *Annu. Rev. Condens. Matter Phys.* **13**, 239 (2022).
- ¹⁷ M. Qin, T. Schäfer, S. Andergassen, P. Corboz, and E. Gull, *Annu. Rev. Condens. Matter Phys.* **13**, 275 (2022).
- ¹⁸ I. Affleck, *Nuclear Physics B* **265**, 409 (1986).
- ¹⁹ I. Affleck, *Nuclear Physics B* **305**, 582 (1988).
- ²⁰ D. S. Rokhsar, *Phys. Rev. B* **42**, 2526 (1990).
- ²¹ M. Marder, N. Papanicolaou, and G. C. Psaltakis, *Phys. Rev. B* **41**, 6920 (1990).
- ²² Y. Q. Li, M. Ma, D. N. Shi, and F. C. Zhang, *Phys. Rev. Lett.* **81**, 3527 (1998).
- ²³ M. G. Yamada, M. Oshikawa, and G. Jackeli, *Phys. Rev. Lett.* **121**, 097201 (2018).
- ²⁴ A. M. Fischer, R. A. Römer, and A. B. Dzyubenko, *Journal of Physics: Conference Series* **286**, 012054 (2011).
- ²⁵ Y.-H. Zhang, D. N. Sheng, and A. Vishwanath, *Phys. Rev. Lett.* **127**, 247701 (2021).
- ²⁶ C. Wu, J.-p. Hu, and S.-c. Zhang, *Phys. Rev. Lett.* **91**, 186402 (2003).
- ²⁷ C. Honerkamp and W. Hofstetter, *Phys. Rev. Lett.* **92**, 170403 (2004).
- ²⁸ C. Wu, *Modern Physics Letters B* **20**, 1707 (2006).
- ²⁹ M. A. Cazalilla, A. F. Ho, and M. Ueda, *New Journal of Physics* **11**, 103033 (2009).
- ³⁰ A. V. Gorshkov, M. Hermele, V. Gurarie, C. Xu, P. S. Julienne, J. Ye, P. Zoller, E. Demler, M. D. Lukin, and A. Rey, *Nature physics* **6**, 289 (2010).
- ³¹ S. Capponi, P. Lecheminant, and K. Totsuka, *Annals of Physics* **367**, 50 (2016).
- ³² E. I.-G.-P. S. Choudhury, *Journal of Physics: Condensed Matter* **37**, 083003 (2024).
- ³³ B. Mukherjee, J. M. Hutson, and K. Hazzard, *New Journal of Physics* (2024).
- ³⁴ D. F. Schroeter, E. Kapit, R. Thomale, and M. Greiter, *Phys. Rev. Lett.* **99**, 097202 (2007).
- ³⁵ M. Hermele, V. Gurarie, and A. M. Rey, *Phys. Rev. Lett.* **103**, 135301 (2009).
- ³⁶ A. E. B. Nielsen, G. Sierra, and J. I. Cirac, *Nature Communications* **4**, 2864 (2013).
- ³⁷ K. Kumar, K. Sun, and E. Fradkin, *Phys. Rev. B* **92**, 094433 (2015).
- ³⁸ P. Nataf, M. Lajkó, A. Wietek, K. Penc, F. Mila, and A. M. Läuchli, *Phys. Rev. Lett.* **117**, 167202 (2016).
- ³⁹ G. Chen, K. R. A. Hazzard, A. M. Rey, and M. Hermele, *Phys. Rev. A* **93**, 061601 (2016).
- ⁴⁰ C. Boos, C. J. Ganahl, M. Lajkó, P. Nataf, A. M. Läuchli, K. Penc, K. P. Schmidt, and F. Mila, *Phys. Rev. Res.* **2**, 023098 (2020).
- ⁴¹ J.-Y. Chen, J.-W. Li, P. Nataf, S. Capponi, M. Mambrini, K. Totsuka, H.-H. Tu, A. Weichselbaum, J. von Delft, and D. Poilblanc, *Phys. Rev. B* **104**, 235104 (2021).
- ⁴² Z.-C. Gu and X.-G. Wen, *Phys. Rev. B* **80**, 155131 (2009).
- ⁴³ X. Chen, Z.-C. Gu, and X.-G. Wen, *Phys. Rev. B* **82**, 155138 (2010).
- ⁴⁴ L. Fidkowski and A. Kitaev, *Phys. Rev. B* **83**, 075103 (2011).
- ⁴⁵ H. Nonne, P. Lecheminant, S. Capponi, G. Roux, and E. Boulat, *Phys. Rev. B* **84**, 125123 (2011).
- ⁴⁶ H. Nonne, M. Moliner, S. Capponi, P. Lecheminant, and K. Totsuka, *EPL (Europhysics Letters)* **102**, 37008 (2013).
- ⁴⁷ K. Duivenvoorden and T. Quella, *Phys. Rev. B* **86**, 235142 (2012).
- ⁴⁸ K. Duivenvoorden and T. Quella, *Phys. Rev. B* **88**, 125115 (2013).
- ⁴⁹ K. Duivenvoorden and T. Quella, *Phys. Rev. B* **87**, 125145 (2013).
- ⁵⁰ K. Tanimoto and K. Totsuka, *arXiv/Condmat* (2015), 1508.07601 [cond-mat.str-el].
- ⁵¹ B. Sutherland, *Physical Review B* **12**, 3795 (1975).
- ⁵² E. H. Lieb and F. Y. Wu, *Phys. Rev. Lett.* **20**, 1445 (1968).
- ⁵³ K. S. D. Beach, F. Alet, M. Mambrini, and S. Capponi, *Phys. Rev. B* **80**, 184401 (2009).
- ⁵⁴ T. C. Lang, Z. Y. Meng, A. Muramatsu, S. Wessel, and F. F. Assaad, *Phys. Rev. Lett.* **111**, 066401 (2013).
- ⁵⁵ J. D'Emidio, M. S. Block, and R. K. Kaul, *Phys. Rev. B* **92**, 054411 (2015).
- ⁵⁶ J. D'Emidio and R. K. Kaul, *Phys. Rev. B* **93**, 054406 (2016).
- ⁵⁷ D. Wang, Y. Li, Z. Cai, Z. Zhou, Y. Wang, and C. Wu, *Phys. Rev. Lett.* **112**, 156403 (2014).
- ⁵⁸ S. Xu, J. T. Barreiro, Y. Wang, and C. Wu, *Phys. Rev. Lett.* **121**, 167205 (2018).
- ⁵⁹ D. E. Rutherford, *Substitutional Analysis* (Edinburgh University Press, 1948).
- ⁶⁰ J. F. Cornwell, *Group Theory in Physics* (Academic Press, 1984).
- ⁶¹ J. P. F. W. Jin-Quan Chen, *Group Representation Theory for Physicists* (World Scientific, 2002).
- ⁶² P. Nataf and F. Mila, *Phys. Rev. Lett.* **113**, 127204 (2014).
- ⁶³ T. Botzung and P. Nataf, *Phys. Rev. Lett.* **132**, 153001 (2024).
- ⁶⁴ T. Botzung and P. Nataf, *Phys. Rev. B* **109**, 235131 (2024).
- ⁶⁵ A. I. Molev, *arXiv* (2002), math/0211289 [math.RT].
- ⁶⁶ A. Young, *Proc. London. Math. Soc.* **2**, 196 (1931).
- ⁶⁷ P. Nataf and F. Mila, *Phys. Rev. B* **97**, 134420 (2018).
- ⁶⁸ S. R. White, *Phys. Rev. Lett.* **69**, 2863 (1992).
- ⁶⁹ S. R. White and D. A. Huse, *Phys. Rev. B* **48**, 3844 (1993).
- ⁷⁰ A. Alex, M. Kalus, A. Huckleberry, and J. von Delft, *Journal of Mathematical Physics* **52**, 023507 (2011), <http://dx.doi.org/10.1063/1.3521562>.
- ⁷¹ F. D. M. Haldane, *Physical Review Letters* **50**, 1153 (1983).
- ⁷² F. D. M. Haldane, *Physics Letters A* **93**, 464 (1983).
- ⁷³ M. Greiter and S. Rachel, *Phys. Rev. B* **75**, 184441 (2007).
- ⁷⁴ S. Rachel, R. Thomale, M. Fuhringer, P. Schmitteckert, and M. Greiter, *Phys. Rev. B* **80**, 180420 (2009).
- ⁷⁵ D. Bykov, *Communications in Mathematical Physics* **322**, 807 (2013).
- ⁷⁶ M. Lajkó, K. Wamer, F. Mila, and I. Affleck, *Nuclear Physics B* **924**, 508 (2017).
- ⁷⁷ Y. Tanizaki and T. Sulejmanpasic, *Phys. Rev. B* **98**, 115126 (2018).
- ⁷⁸ Y. Yao, C.-T. Hsieh, and M. Oshikawa, *Phys. Rev. Lett.* **123**, 180201 (2019).
- ⁷⁹ K. Wamer, M. Lajkó, F. Mila, and I. Affleck, *Nuclear Physics B* **952**, 114932 (2020).
- ⁸⁰ P. Nataf, S. Gozel, and F. Mila, *Phys. Rev. B* **104**, L180411 (2021).
- ⁸¹ I. Affleck, *Phys. Rev. Lett.* **56**, 746 (1986).
- ⁸² T. Ziman and H. J. Schulz, *Phys. Rev. Lett.* **59**, 140 (1987).
- ⁸³ K. Ohmori, N. Seiberg, and S.-H. Shao, *SciPost Phys.* **6**, 017 (2019).
- ⁸⁴ P. Lecheminant, *Nuclear Physics B* **901**, 510 (2015).
- ⁸⁵ S. Gozel, P. Nataf, and F. Mila, *Phys. Rev. Lett.* **125**, 057202 (2020).
- ⁸⁶ P. Fromholz and P. Lecheminant, *Phys. Rev. B* **102**, 094410 (2020).
- ⁸⁷ L. Devos, L. Vanderstraeten, and F. Verstraete, *Phys. Rev. B* **106**, 155103 (2022).
- ⁸⁸ V. Zauner-Stauber, L. Vanderstraeten, M. T. Fishman, F. Verstraete, and J. Haegeman, *Phys. Rev. B* **97**, 045145 (2018).

- ⁸⁹ I. M. Gelfand and M. L. Tsetlin, Dokl. Akad. Nauk SSSR **71**, 825 (1950).
- ⁹⁰ R. Assaraf, P. Azaria, M. Caffarel, and P. Lecheminant, Phys. Rev. B **60**, 2299 (1999).
- ⁹¹ K. Pilch and A. N. Schellekens, Journal of Mathematical Physics **25**, 3455 (1984).
- ⁹² N. J. Vilenkin and A. U. Klimyk, *Representation of Lie groups and special functions, Vol. 3* (Kluwer Academic Publishers, 1992).
- ⁹³ C. Itzykson and M. Nauenberg, Rev. Mod. Phys. **38**, 95 (1966).
- ⁹⁴ G. Sierra and T. Nishino, Nuclear Physics B **495**, 505 (1997).
- ⁹⁵ A. Weichselbaum, Annals of Physics **327**, 2972 (2012).
- ⁹⁶ Equivalently, the shapes before transposition represent the same $SU(N)$ irreps independently of the empty N -boxes column that one could add/withdraw, since we calculate $SU(N)$ group theory coefficients.
- ⁹⁷ P. Nataf and F. Mila, Phys. Rev. B **93**, 155134 (2016).
- ⁹⁸ A. Weichselbaum, Phys. Rev. Res. **2**, 023385 (2020).
- ⁹⁹ I. P. McCulloch and M. Gulácsi, EPL (Europhysics Letters) **57**, 852 (2002).
- ¹⁰⁰ I. P. McCulloch, Journal of Statistical Mechanics: Theory and Experiment **2007**, P10014 (2007).
- ¹⁰¹ L. C. Biedenharn and J. D. Louck, *Angular Momentum in Quantum Physics: Theory and Application* (Addison-Wesley Publishing Company, 1981).
- ¹⁰² P. Kramer, Zeitschrift für Physik A Hadrons and nuclei , 68 (1968).
- ¹⁰³ P. Dang, J. P. Draayer, F. Pan, and K. S. Becker, The European Physical Journal Plus , 704 (2024).
- ¹⁰⁴ Note that gauge issues also exist when $T_{N_s+1}^{\tilde{\gamma}L}(q_1, q_2) = 1$. For instance, in Eq. 18, one could multiply all the coefficients of the RHS by -1 . Again, the requirement is to stay consistent (by imposing for instance positive sign for the coefficient of the *largest* SSYT of the linear superposition).
- ¹⁰⁵ Note that the two limits do not commute exactly, but the difference for $\Delta_c(m = +\infty, L = +\infty)$ is irrelevant ($\lesssim 1e-3$) and does not change our estimate of U_c .
- ¹⁰⁶ S. R. Manmana, K. R. A. Hazzard, G. Chen, A. E. Feiguin, and A. M. Rey, Phys. Rev. A **84**, 043601 (2011).
- ¹⁰⁷ K. Buchta, O. Legeza, E. Szirmai, and J. Sólyom, Phys. Rev. B **75**, 155108 (2007).
- ¹⁰⁸ P. Calabrese and J. Cardy, Journal of Statistical Mechanics: Theory and Experiment **2004**, P06002 (2004).
- ¹⁰⁹ N. Laflorencie, E. S. Sørensen, M.-S. Chang, and I. Affleck, Phys. Rev. Lett. **96**, 100603 (2006).
- ¹¹⁰ S. Capponi, P. Lecheminant, and M. Moliner, Phys. Rev. B **88**, 075132 (2013).
- ¹¹¹ M. Fuhringer, S. Rachel, R. Thomale, M. Greiter, and P. Schmitteckert, Annalen der Physik **17**, 922 (2008).
- ¹¹² E. Szirmai, O. Legeza, and J. Sólyom, Phys. Rev. B **77**, 045106 (2008).
- ¹¹³ I. Affleck, D. Gepner, H. J. Schulz, and T. Ziman, Journal of Physics A: Mathematical and General **22**, 511 (1989).
- ¹¹⁴ C. J. Hamer, G. R. W. Quispel, and M. T. Batchelor, Journal of Physics A: Mathematical and General **20**, 5677 (1987).
- ¹¹⁵ I. Affleck and S. Qin, Journal of Physics A: Mathematical and General **32**, 7815 (1999).
- ¹¹⁶ R. Assaraf, P. Azaria, E. Boulat, M. Caffarel, and P. Lecheminant, Phys. Rev. Lett. **93**, 016407 (2004).
- ¹¹⁷ J. Zhao, K. Ueda, and X. Wang, Phys. Rev. B **74**, 233102 (2006).
- ¹¹⁸ P. Lecheminant and A. M. Tsvelik, Phys. Rev. B **91**, 174407 (2015).
- ¹¹⁹ A. Weichselbaum, S. Capponi, P. Lecheminant, A. M. Tsvelik, and A. M. Läuchli, Phys. Rev. B **98**, 085104 (2018).
- ¹²⁰ S. Capponi, P. Fromholz, P. Lecheminant, and K. Totsuka, Phys. Rev. B **101**, 195121 (2020).
- ¹²¹ R. Bondesan and T. Quella, Nuclear Physics B **886**, 483 (2014).
- ¹²² S. Capponi, L. Devos, P. Lecheminant, K. Totsuka, and L. Vanderstraeten, “Non-landau quantum phase transition in modulated $su(n)$ heisenberg spin chains,” (2024), 2409.01019 [cond-mat.str-el].
- ¹²³ B. Bruognolo, J.-W. Li, J. von Delft, and A. Weichselbaum, SciPost Phys. Lect. Notes , 25 (2021).
- ¹²⁴ A. Weichselbaum, SciPost Phys. Codebases , 40 (2024).
- ¹²⁵ L. Vanderstraeten, J. Haegeman, and F. Verstraete, SciPost Phys. Lect. Notes , 7 (2019).
- ¹²⁶ M. Fishman, S. R. White, and E. M. Stoudenmire, SciPost Phys. Codebases , 4 (2022).
- ¹²⁷ K. Kobayashi, M. Okumura, Y. Ota, S. Yamada, and M. Machida, Phys. Rev. Lett. **109**, 235302 (2012).
- ¹²⁸ V. Bois, S. Capponi, P. Lecheminant, M. Moliner, and K. Totsuka, Phys. Rev. B **91**, 075121 (2015).
- ¹²⁹ H. Katsura, T. Hirano, and V. E. Korepin, Journal of Physics A: Mathematical and Theoretical **41**, 135304 (2008).
- ¹³⁰ R. Abhishek and T. Quella, ArXiv e-prints (2015), arXiv:1512.05229.
- ¹³¹ J. Dufour, P. Nataf, and F. Mila, Phys. Rev. B **91**, 174427 (2015).
- ¹³² K. Wan, P. Nataf, and F. Mila, Phys. Rev. B **96**, 115159 (2017).
- ¹³³ A. Roy and T. Quella, Phys. Rev. B **97**, 155148 (2018).
- ¹³⁴ S. Gozel, D. Poilblanc, I. Affleck, and F. Mila, Nuclear Physics B (2019).
- ¹³⁵ L. Herviou, A. Rey, and F. Mila, arXiv/Condat (2024), 2411.17848 [cond-mat.str-el].
- ¹³⁶ T. Morimoto, H. Ueda, T. Momoi, and A. Furusaki, Phys. Rev. B **90**, 235111 (2014).